photonics

MDPI

Review

Fiber-Optic Sensor Technologies for Concrete Structural Health Monitoring: Measurement Chains, Interrogation Approaches, and Research Trends

Ugis Senkans [1,2], Janis Braunfelds [1,2,*], Rihards Gailitis [3], Andina Sprince [3], Sandis Spolitis [1,4] and Vjaceslavs Bobrovs [1]

[1] Institute of Photonics, Electronics and Telecommunications, Riga Technical University, Azenes Street 12, LV-1048 Riga, Latvia; ugis.senkans@rtu.lv (U.S.); sandis.spolitis@rtu.lv (S.S.); vjaceslavs.bobrovs@rtu.lv (V.B.)
[2] Fiber Optical Sensor Research Group (RTU FiberSens), Riga Technical University, Azenes Street 12, LV-1048 Riga, Latvia
[3] Institute of High-Performance Materials and Structures, Riga Technical University, Kipsalas 6a, LV-1048 Riga, Latvia; rihards.gailitis@rtu.lv (R.G.); andina.sprince@rtu.lv (A.S.)
[4] RTU Communication Technologies Research Center (RTU ComTech), Riga Technical University, Azenes Street 12, LV-1048 Riga, Latvia
* Correspondence: janis.braunfelds@rtu.lv

Abstract

Fiber-optic sensing supports measurements of strain, temperature, cracking, and durability in concrete structural health monitoring (SHM). This review compares fiber Bragg grating (FBG), Fabry-Pérot, Rayleigh optical frequency-domain reflectometry (OFDR), Brillouin and Raman distributed systems, polymer optical fibers, and optical chemical sensors across the measurement chain, from optical response and interrogation to engineering quantities and validation. A curated technical synthesis is complemented by a Scopus map of 3100 source records from three technology and civil-infrastructure query families (2015–2026; 2026 partial). Annual records rose from 145 in 2015 to 451 in 2025. FBG terminology rose from 89 to 182 records over the same period, while its share of annual records declined from 61.4% to 40.4%. The reviewed studies show why wavelength sensitivity, sensing range, and sampling interval cannot substitute for validated accuracy in concrete: temperature compensation, cable construction, strain transfer, processing length, and the reference measurement affect the recovered quantity. OFDR and distributed acoustic sensing are counted separately in the terminology map. The comparison identifies the configuration and reporting details needed to assess these methods for concrete monitoring.

Keywords: fiber-optic sensors; fiber Bragg grating; distributed fiber-optic sensing; optical frequency-domain reflectometry; Brillouin sensing; optical interrogation; structural health monitoring; concrete structures

Check for updates

Received: 30 September 2026
Revised: 17 November 2026
Accepted: 19 November 2026
Published: 21 November 2026

Copyright: © 2026 by the authors. Licensee MDPI, Basel, Switzerland. This article is an open access article distributed under the terms and conditions of the Creative Commons Attribution (CC BY) license.

1. Introduction

Fiber-optic sensing has been applied to civil engineering and concrete structural health monitoring (SHM) for several decades, from early concrete-specific implementations to modern multiplexed fiber Bragg grating (FBG) networks and fully distributed sensing systems [1–4]. Fiber-optic sensors offer several characteristics relevant to these applications, including small dimensions, passive operation at the sensing location, immunity to electromagnetic interference, remote interrogation, and the possibility of multiplexing

several sensing points along a single optical fiber [2,4–7]. In concrete structures, these characteristics support strain and temperature monitoring, crack-related measurements, dynamic response assessment, and long-term structural monitoring [2,4,8].

The reviewed technologies share optical fiber as the sensing or transmission medium, but their operating principles and measurement characteristics differ considerably. FBG sensors encode strain- and temperature-induced changes mainly as a Bragg-wavelength shift, whereas interferometric sensors use optical phase or cavity-length changes [5–7]. Distributed Rayleigh- and Brillouin-based systems recover spatially resolved information from backscattered light, while Raman systems are used mainly for distributed temperature measurements [4,9–11]. Polymer optical fibers (POFs) extend the measurement space toward larger deformation and mechanically compliant sensing. A 2026 systematic review identifies intensity-modulated sensing as the dominant POF approach in SHM, with OTDR-based distributed methods forming a smaller subset [12]. Fiber-optic chemical sensors have been demonstrated for pH- and chloride-related measurements in cementitious materials [13–18]. System performance depends on both the sensing element and the method used to interrogate and process its optical response.

Interrogation and signal processing determine the usable resolution, sensing range, acquisition rate, optical power budget, multiplexing capacity, and system stability. FBG interrogation methods differ in wavelength resolution, acquisition rate, stability, complexity, and channel capacity [5–7]. In distributed sensing, the sensing range, effective spatial resolution, and acquisition time depend on the selected interrogation architecture and processing method [10,11]. These system-level parameters are considered together with the sensing principle and the structural measurand.

Recent reviews differ in host material and analytical focus. Golovastikov et al. [2] survey optical sensing across civil and urban infrastructure, while the earlier review by Senkans et al. [4] compares FBG and Rayleigh-, Brillouin-, and Raman-based sensing for road infrastructure. FBG-focused reviews cover grating sensors and interrogation [5–7]; other syntheses focus on distributed crack monitoring [8,19], concrete durability [20], or dams [21]. The present review extends the road-focused comparison to concrete structures and considers Fabry–Pérot, polymer, and chemical sensors alongside the distributed families. Its common basis is the complete chain from optical observables and interrogation to the recovered structural or environmental quantity and the evidence used to validate it.

The present review develops this comparison through a measurement-chain framework. FBG and interferometric sensors, Rayleigh-, Brillouin-, and Raman-based distributed methods, polymer optical fibers, and durability-oriented optical sensors are compared from the sensing mechanism through interrogation and signal processing to the structural or environmental quantity used for SHM interpretation. The comparison focuses on network scalability, spatial coverage, range–resolution–speed trade-offs, calibration and compensation, strain transfer, validation metrics, and evidence level. Reported performance is considered alongside the conditions under which each technology was tested in concrete structures.

2. Review Design, Search Scope, and Data Basis

The review is organized around three questions. First, what physical quantity is measured by each fiber-optic architecture and how is it recovered through interrogation and processing? Second, which performance descriptors and validation methods allow meaningful comparison across sensor families? Third, which limitations currently constrain translation from laboratory demonstration to concrete-SHM deployment? The technical synthesis supports statements about sensing performance and validation. The Scopus mapping characterizes publication activity and terminology within the specified query

domain. Section 6.3 interprets the two layers together using the validation criteria in Section 6.2 without assigning a numerical maturity score to technology families.

2.1. Review Design and Evidence Synthesis

The technical synthesis is based on a structured but deliberately non-exhaustive literature identification procedure. Candidate studies were identified in Scopus by combining sensing-technology terms (FBG, Fabry–Pérot (FP), OFDR, Rayleigh, Brillouin, Brillouin Optical Time-Domain Analysis (BOTDA), Brillouin Optical Time-Domain Reflectometry (BOTDR), Brillouin Optical Correlation-Domain Analysis (BOCDA), Raman DTS, polymer optical fiber, long-period grating) with host-material terms (concrete, reinforced concrete, prestressed concrete, cementitious, mortar) and monitoring terms (structural health monitoring, strain, crack, corrosion, durability). Identification was complemented by backward and forward citation tracking from the most recent technology-specific reviews [2,5–8,19,20,22–24] and by targeted retrieval of photonic instrumentation studies that are not indexed under concrete-related terms but define the interrogation and network constraints analyzed in Section 4.

Studies were retained when they reported the sensing element or cable and its coupling to the host, the interrogation principle together with the settings relevant to the reported values, and a measured structural, thermal or environmental quantity with an identifiable validation basis. Studies were excluded when the measurement configuration could not be reconstructed from the text, when reported performance could not be attributed to a defined interrogation and processing chain, or when the work repeated an earlier report by the same group without new measurement evidence.

This procedure is reported as a structured narrative synthesis rather than as a systematic review. The objective is not to establish the prevalence of findings across the literature, which would require exhaustive and protocol-driven retrieval, but to compare a defined set of technologies within a common measurement-chain framework. The quantitative mapping described in Section 2.2 therefore uses an independent, fully specified, and reproducible search, and the two evidence layers are kept methodologically separate for this reason. The technical evidence covers fiber-optic sensing in concrete, reinforced concrete, prestressed concrete, and related cementitious structures. Current performance and validation are characterized primarily from recent primary studies and reviews. Foundational studies establish sensing principles, interrogation methods, and early concrete applications. Studies outside concrete inform transferable photonic methods, including interrogation, multiplexing, optical-network scaling, and signal processing. Concrete-specific performance is evaluated from studies in cementitious structures.

Each sensing approach is compared using the optical observable, interrogation and network arrangement, measured structural or environmental quantity, sensing range or spatial coverage, spatial resolution where applicable, acquisition or update behavior, calibration and compensation requirements, cross-sensitivity, and validation metric. Reported numerical values are treated as configuration-dependent because interrogator settings, fiber and coating, gauge or processing length, installation and bonding, specimen scale, and loading or exposure conditions can alter the recovered response. Performance values are reported with the sensor configurations and measurement conditions that produced them.

2.2. Scopus Mapping Dataset

The quantitative mapping is based on three Scopus searches frozen on 26 August 2026: FBG/grating sensing (S-FBG-01), distributed sensing using Rayleigh, Brillouin, Raman, and related reflectometric methods (S-DFOS-01), and a targeted long-gauge supplement (S-LGFOS-01). Each search combined sensing terms with a host-material and

civil-infrastructure term block, covering concrete and cementitious materials as well as broader settings such as roads, bridges, dams, and geotechnical works. The dataset therefore describes the retrieved civil-infrastructure sensing domain, not only studies performed in concrete. It covers English-language journal articles, full conference papers, indexed book chapters, and reviews from 2015 to 2026. Exact queries and export counts are in Supplementary Table S1; the 2026 data include records indexed through 26 August and are treated as a partial year.

The three exports contained 3256 rows: 1524 from S-FBG-01, 1696 from S-DFOS-01, and 36 from S-LGFOS-01. Counting an EID appearing in more than one export, we removed 139 repeated appearances and left 3117 distinct EIDs. The identity audit then removed 17 further duplicate rows: six pairs shared a normalized DOI, and 11 pairs had the same normalized title, year, and document type without a conflicting DOI. The more complete row was retained in each case. This yielded 3100 source-level records for annual and terminology statistics. Two other pairs refer to the same publications but were retained as separate source rows to preserve their different indexing metadata: one proceeding paper has different source labels and years, and one ETOP 2025 paper has two publisher/DOI records. Counting each pair once gives 3098 canonical publications. Excluding the two alias rows instead would change the 2018 and 2025 annual totals from 206 to 205 and from 451 to 450, respectively. The 2025 FBG share would change from 40.4% to 40.2%. Trends are reported for the 3100 source rows, and the 3098 count is used only for publication identities.

The mapping describes records returned by the specified technology and civil-infrastructure queries. Term frequency measures the vocabulary of that corpus, not technology prevalence across all concrete-SHM publications. Interferometric, polymer-optical-fiber, and chemical sensors are treated in the technical synthesis. Their incidental occurrence in mapped records is not a separate search-based comparison. Table 1 reports the source-record accounting and document types.

Table 1. Characteristics of the Scopus mapping dataset.

Descriptor	Value	Interpretation
Raw Scopus export rows	3256	Rows from the three exports before repeated EIDs were counted once
Unique Scopus EIDs	3117	After removal of 139 repeated EIDs occurring across query exports
Source-level mapping records	3100	Six normalized-DOI matches and 11 matching title/year/document-type rows; the more complete bibliographic row was retained
Unique publications	3098	Two pairs of source records refer to the same publications; each pair is counted as one publication
Journal articles	1982 (63.9%)	Main document type in the mapping dataset
Conference papers	979 (31.6%)	Conference contribution to the mapping dataset
Reviews	79 (2.5%)	Secondary literature in the mapping dataset
Book chapters	60 (1.9%)	Minor document type in the mapping dataset
Records with DOI	91.16%	Identity checking and publication reconciliation
2026 records	318	Partial year; excluded from complete-year comparison

Annual percentages use all mapped source records assigned to that year as the denominator: for example, the 2015 FBG-based share is 89/145, and the 2025 share is 182/451. A record contributes at most once to a term group, but may contribute to several groups, so the shares may sum to more than 100%. The archived generic distributed-sensing group records broad wording such as distributed fiber-optic sensing (DFOS) and DOFS. Therefore, it does

not identify a particular scattering method. To distinguish OFDR from distributed acoustic sensing (DAS) within the previously combined Rayleigh/OFDR/DAS term group, two additional, non-exclusive flags were calculated from titles, abstracts, author keywords, and index keywords of the 3100 retained records. The OFDR flag matches OFDR or the phrase optical frequency-domain reflectomet*; the DAS flag matches DAS, distributed acoustic sens*/detect*, phase-sensitive or coherent optical time-domain reflectomet*, or phi-OTDR. Rayleigh wording alone is not counted as OFDR. A record containing both explicit families receives both flags. The original combined 400-record signal remains documented in Supplementary Table S1 as an archived category. The explicit flags are reported separately in Section 6.1.

Figure 1 outlines the review framework, showing the technical literature synthesis, Scopus mapping, and their use in the analysis of fiber-optic sensing for concrete SHM. The technical literature supports the comparison of sensing principles, interrogation and processing, measured quantities, and validation in Sections 3–5; the Scopus mapping describes publication and terminology trends in Section 6.

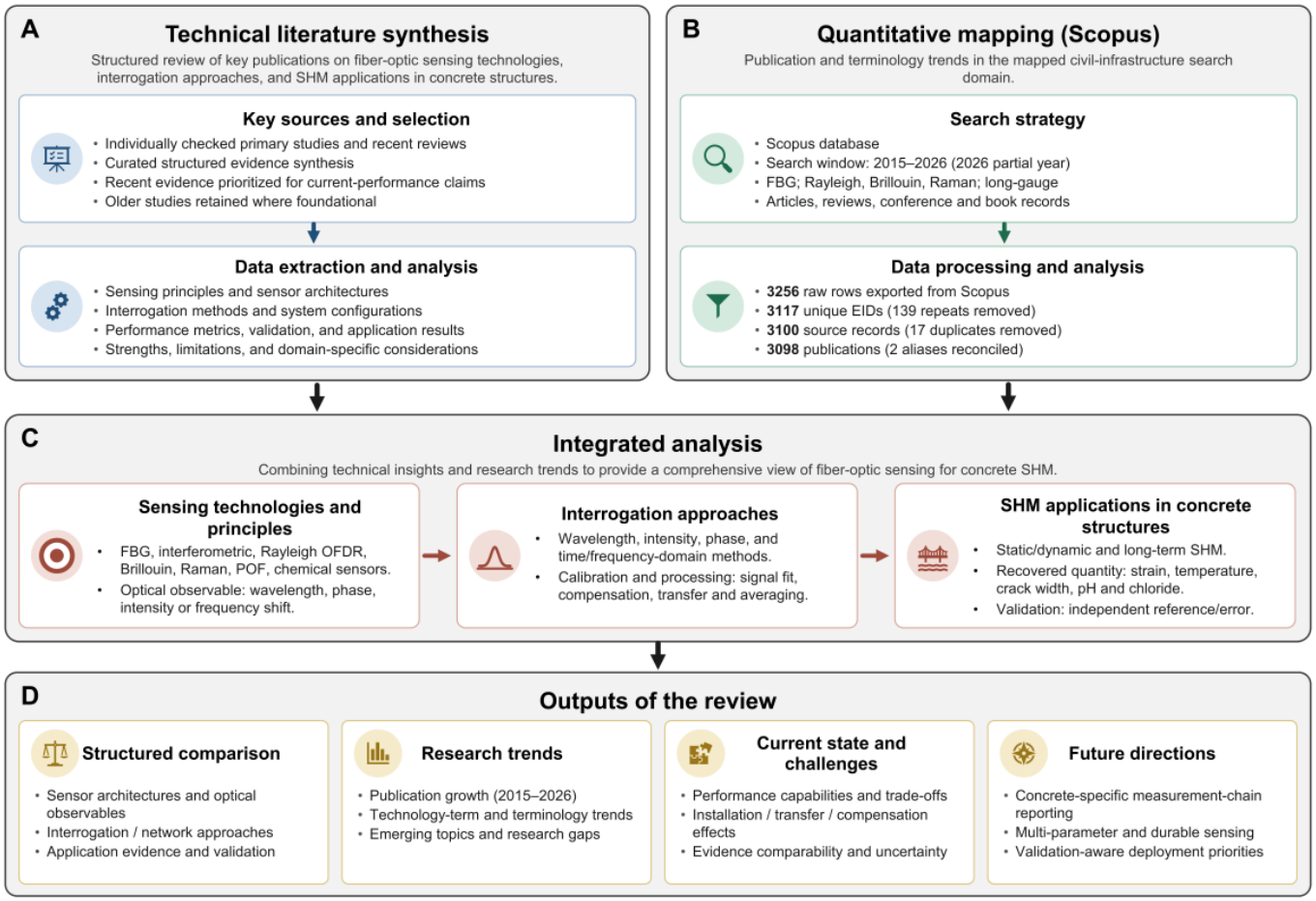


Figure 1. Review framework separating the curated technical literature synthesis from the quantitative Scopus mapping layer and showing how both streams are brought together in the comparison of publication visibility and validation depth in Section 6.3. Data processing and analysis are shown in Supplementary Table S1.

3. Fiber-Optic Sensor Technologies for Concrete SHM

Concrete SHM uses sensor technologies with different transduction principles, spatial coverage, interrogation requirements, and measurable quantities. The following comparison is organized by sensing function: (1) discrete and quasi-distributed FBG and interferometric

sensors, (2) distributed Rayleigh, Brillouin, and Raman methods, and (3) polymer and durability-oriented optical sensors.

3.1. Fiber Bragg Grating and Interferometric Sensors

Fiber Bragg grating (FBG) sensors are one of the most established discrete optical sensing technologies used in structural health monitoring. An FBG consists of a periodic modulation of the effective refractive index along the fiber core. The reflected Bragg wavelength is defined by $\lambda_B = 2\, n_{eff}\Lambda$, where n_{eff} is the effective refractive index, and Λ is the grating period. Axial strain and temperature change one or both terms and shift the reflected wavelength [5]. Because the measurand is primarily encoded in wavelength rather than absolute optical power, FBG measurements are comparatively robust against source-power fluctuations and transmission loss, provided that the reflection peak remains detectable and correctly resolved [5]. The same wavelength response is affected by both strain and temperature, so temperature compensation is required when mechanical strain is the target quantity [5]. To first order, the Bragg-wavelength shift (Equation (1)) contains contributions from both strain and temperature:

$$\Delta\lambda_B = k_\varepsilon\, \varepsilon + k_T\, \Delta T \tag{1}$$

with an independently measured temperature change, mechanical strain (Equation (2)) is then calculated as

$$\varepsilon = (\Delta\lambda_B - k_T\, \Delta T)/k_\varepsilon \tag{2}$$

where k_ε is the calibrated mechanical strain coefficient, and k_T is the temperature coefficient, incorporating thermo-optic and thermal-expansion effects for the installed grating [5,7]. At fixed temperature, a wavelength uncertainty u_λ contributes approximately $u_\lambda/|k_\varepsilon|$ to strain uncertainty. An independent temperature-reference uncertainty u_T contributes approximately $|k_T/k_\varepsilon|u_T$; coefficient calibration and strain transfer add further contributions. A mechanically isolated or co-located thermal reference is therefore required to interpret the compensated shift as mechanical strain.

FBG sensing remains one of the most mature point and quasi-distributed optical approaches for civil SHM. Yassin et al. report wavelength-dependent FBG strain responsivities of approximately 0.64–1.2 pm/με and reviewed vibration implementations extending to at least 20 kHz [6]. The responsivity range is a transduction coefficient rather than a system-accuracy specification, while usable dynamic bandwidth depends on the interrogator and processing chain [6,7]. Recent concrete-specific work includes reinforcing-bar slippage and bond-slip characterization with FBG displacement sensors [25], road-infrastructure monitoring with embedded FBG networks [26,27], and optical-fiber-instrumented prestressing strands for force measurement [28]. The practical measurement framework is thus set by the grating, packaging, wavelength allocation, interrogator, and temperature-compensation strategy.

FBG arrays commonly use wavelength-division multiplexing, with gratings at different nominal Bragg wavelengths placed along one optical fiber to provide quasi-distributed measurements [5]. This configuration has also been considered for road-infrastructure monitoring [26]. The usable sensor count is jointly limited by the available spectral band, expected strain- and temperature-induced wavelength excursion, reflection bandwidth, grating reflectivity, optical loss, and the ability of the interrogator to resolve adjacent peaks [5]. FBG sensor design and network design are closely linked through the available wavelength and power budgets.

Interferometric fiber sensors, including intrinsic and extrinsic Fabry–Pérot (FP) configurations, form another group of discrete optical sensors. Their response is obtained from changes in optical phase or cavity length rather than from a Bragg wavelength shift.

Concrete-specific FP studies are mainly foundational demonstrations of embedded or reinforcement-coupled local strain sensing [29,30]. These studies support comparison of sensing principles, interrogation requirements, multiplexing, and validation needs, while their historical test configurations do not establish current numerical performance limits.

FBG and FP systems serve different measurement architectures. FBGs are well suited to wavelength-multiplexed arrays with multiple discrete sensing locations on one fiber, whereas FP configurations remain useful for dedicated local measurements that justify cavity-based interrogation [5,7,29,30]. In concrete SHM, selection is governed primarily by the required sensing locations, multiplexing scale, interrogator architecture, installation constraints, and validation method.

3.2. Distributed Rayleigh, Brillouin, and Raman Sensing

Fully distributed fiber-optic sensing (DFOS) recovers spatial information from backscattered light along the sensing fiber rather than from predefined sensor locations. Position is encoded through propagation time, optical frequency, or a controlled correlation condition, depending on the interrogation method. Rayleigh-, Brillouin-, and Raman-based systems share the fiber as a sensing medium but differ in observable, range, spatial resolution, acquisition time, and measurand [9–11,22–24,31,32].

Brillouin sensing responds to both mechanical strain and temperature through a shift of the Brillouin spectral peak. BOTDR measures spontaneous backscatter from one end of the fiber, while BOTDA interrogates stimulated interaction between counter-propagating waves and normally requires both fiber ends [4,32]. Reviews report long conventional sensing lengths and shorter-range, finer resolution research configurations under different conditions [22–24]. BOCDA selects a localized correlation peak for fine spatial measurements over architecture-dependent lengths [11,22].

The fitted Brillouin spectral peak frequency is the optical result. Under a local calibration, its change can be written as follows [4,32,33]:

$$\Delta\nu_B = C_\varepsilon\,\varepsilon + C_T\,\Delta T \tag{3}$$

the coefficients C_ε and C_T depend on the fiber and calibration conditions. A measured peak shift cannot be assigned to mechanical strain without independent temperature information or a calibrated multi-parameter procedure. Spectral fitting, spatial averaging, and scan time determine the uncertainty and effective update rate of the resulting profile [32,33].

Recent civil-engineering studies have focused on deployment, compensation, and long-term strain transfer. Brillouin sensing has been used to evaluate tendon-force distribution in prestressed concrete bridges [34], to monitor corrosion-related deformation together with FBG measurements [35] and, more recently, to obtain simultaneous distributed strain and temperature information in a mass-concrete raft foundation using BOTDR with a temperature-dependent compensation model [33]. The sensing cable remains part of the measurement chain because coating and mechanical construction control strain transfer [36]. Environmental durability and installation survival therefore require validation separately from interrogator specifications, as demonstrated in recent cable-aging and concrete-embedment studies [33,37,38].

Rayleigh-based distributed sensing interrogated by optical frequency-domain reflectometry (OFDR) uses the local Rayleigh backscatter pattern as a reproducible spectral signature. A swept-frequency measurement maps the backscattered response along the fiber, and local spectral changes between a reference state and a later measurement can be converted to strain or temperature [31,39–41]. Concrete applications have demonstrated crack detection and localization as well as crack-width interpretation [40,42–44], assessment and visualization of reinforced-concrete performance indicators [45], two-dimensional

strain or crack-pattern measurements in disturbed regions [46,47], restrained-shrinkage assessment [48], monitoring of internal swelling processes [49], and combined use with digital image correlation or FBG sensing [50,51]. Recent reviews now consolidate crack-oriented DFOS evidence around three quantitative tasks—crack detection, localization, and crack-width evolution—and emphasize installation method and strain-transfer assumptions as major determinants of quantitative accuracy [8,19]. Current primary studies extend this evidence toward automated crack evaluation [52], restrained-shrinkage and crack monitoring in ultra-high-performance concrete (UHPC) with sub-millimeter OFDR sampling [53], and impact-loaded cementitious specimens, where embedded OFDR sensing localized cracks within 2 mm and estimated crack opening displacement within ±10% under the reported test conditions [54]. Comparative assessment of OFDR measurements requires validated localization and crack-width error together with gauge or processing length, strain transfer, and signal quality.

For Rayleigh/OFDR measurements, sampling interval, gauge or processing length, and effective structural resolution describe different quantities. Output spacing is the distance between reported samples. Processing length is the fiber segment used to estimate a local spectral shift. A longer processing length can improve the correlation quality but averages a larger portion of the strain field [31]. At a crack, deformation is transmitted through the concrete-adhesive-coating-fiber system before optical averaging. Shear-lag descriptions assume elastic layers and continuous bonding. Debonding, slip, cracking, and nonlinear coatings can violate those assumptions [38,55–57]. The resulting peak height and width depend on cable construction, adhesive, bond length, and interrogation settings, so optical sampling density alone does not establish crack-location or crack-width accuracy [8,19,58].

Raman distributed temperature sensing (DTS) recovers temperature from the temperature-dependent anti-Stokes signal relative to a Stokes reference [9]. It contributes to crack-related monitoring by measuring thermal gradients or supplying temperature information for compensation. Thus, Raman DTS is not a direct mechanical crack-width measurement. Brillouin sensing can recover strain after temperature separation, but its spatial averaging also limits the interpretation of local cracks. In a primary concrete-dam study, a Raman DTS configuration had 1.02 m spatial resolution, 0.5 °C temperature resolution, and a minimum acquisition interval of 10 s, with three co-located digital thermometers used to assess a reconstructed temperature field [59]. It is also important to note that the temperature resolution is not the same as validated temperature accuracy. A full-scale facility study with fiber embedded in concrete walls identified calibration, spatial dispersion, and fiber position as dominant contributions to Raman measurement uncertainty [60].

3.3. Polymer Optical Fibers and Fiber-Optic Sensors for Durability Parameters

Polymer optical fibers differ from silica fibers in both mechanical and optical behavior. Their lower stiffness and high deformation tolerance make them attractive for large-strain and crack-related monitoring, while higher attenuation, viscoelasticity, temperature sensitivity, and packaging requirements remain important limitations. A 2026 systematic review of 90 SHM publications identifies intensity-modulated POF sensors as the dominant approach (67% of reviewed studies), followed by OTDR-based distributed POF sensing (14%), and concludes that large-strain monitoring remains one of the principal application strengths [12]. In concrete and civil-engineering applications, POF sensing has been used for cumulative deformation [61] and corrosion-related mechanical response [62]. Accordingly, POF performance is more meaningfully characterized by deformation capacity, field packaging, repeatability, and environmental dependence than by strain limits reported in early POF-FBG demonstrations.

Fiber-optic durability sensors convert local chemical or environmental changes into optical intensity, fluorescence, wavelength, resonance, or spectral variations. The recent durability-focused literature covers FBG, long-period grating (LPFG), fluorescence, surface plasmon resonance (SPR), and distributed optical approaches for pH, ion ingress, carbonation, moisture, and corrosion-related monitoring [20]. For concrete-relevant alkalinity, researchers have applied ratiometric fluorescence to hydroxide-diffusion measurements in cementitious materials [14] and have also investigated hydrogel-coupled FBG transducers for combined pH and strain sensing [15]. Chloride sensing has advanced to a fluorescent fiber-optic probe validated in cement paste at chloride concentrations of 0.001–0.3 M [18]. Earlier concrete chemical-sensor demonstrations [13,16,17] provide methodological background. Their reported performance reflects the instruments and test conditions of those studies.

Carbonation and humidity monitoring use several optical transduction mechanisms. Recent in situ work monitored cement-paste carbonation with embedded multimode-fiber probes, producing a reflected-intensity response associated with $CaCO_3$ formation and demonstrating operation under accelerated CO_2 exposure [63]. Fiber-optic devices have also been developed for relative-humidity measurement in civil structures [64]. In the distributed humidity system of Chow et al. [65], the demonstrated sensing length was approximately 0.5 m. Duplicate calibrated measurements differed by less than 1% RH, while a 65-point moving average corresponding to about 1 cm of fiber was used to obtain a reproducible spatial humidity profile. Earlier Raman-based carbonation profiling [66] demonstrated the sensing principle with device dimensions and excitation settings specific to its experimental configuration. Embedded humidity sensors require packaging that protects the optical element while still permitting moisture transport to the sensing region, and the packaging can affect response time and calibration [67].

Corrosion sensors can be separated by the physical quantity that produces the optical response. Recent examples include Fe-C-coated polymer optical fibers [68] and iron-carbon-coated long-period gratings [69], in which corrosion-sensitive layers modify transmission or resonance as the material state changes. Zhou et al. evaluated a gold-sputtered LPG with an iron-carbon layer during 312 h of immersion in simulated concrete pore solution while recording optical spectra and electrochemical measurements in parallel [69]. Current durability reviews distinguish direct corrosion-sensitive optical transduction from indirect measurement of corrosion-induced mechanical response and identify calibration, selectivity, sensor life, and field validation as key performance considerations [20]. Quantitative comparison therefore requires the calibration variable to match the transduction mechanism and the monitored stage of deterioration.

Polymer and durability-oriented optical sensors cannot be characterized by sensitivity alone. For POF-based SHM, relevant performance descriptors include attenuation, repeatability, hysteresis or creep, temperature dependence, packaging, and field survivability [12]. Chemically functionalized sensors additionally require a defined calibration range, selectivity and cross-sensitivity, response and recovery time, drift, fabrication reproducibility, and ageing assessment, including changes after embedment in cementitious media [13–18,20,63–69]. Table 2 summarizes the principal sensing mechanisms, implementation modes, concrete-SHM measurands, and comparison constraints used in the cross-technology analysis.

Table 2. Comparison of the main photonic sensing principles considered for concrete SHM.

Sensor Technology	Optical Observable/ Interrogation Basis	Spatial Form/Representative Reported Scale	Main SHM Quantities	Main Photonic-System Limitation
FBG	Bragg wavelength shift	Discrete/quasi-distributed. Recent civil-engineering review literature reports wavelength-dependent FBG strain responsivity of approximately 0.64–1.2 pm/με [6]. Reviewed vibration implementations extend to at least ~20 kHz, but usable bandwidth is interrogator- and processing-dependent [6,7].	Strain, temperature, force, dynamic response	Spectral allocation, strain–temperature cross-sensitivity, interrogator resolution and dynamic range
Fabry-Pérot/ interferometric	Phase or cavity-length change	Discrete/local. Phase- or cavity-based point sensing with performance strongly dependent on cavity design and interrogation architecture [7].	High-resolution local strain/ displacement	Multiplexing and phase/cavity interrogation complexity
Brillouin BOTDA/BOTDR	Brillouin frequency shift	Fully distributed strain and temperature. Range and spatial resolution vary with configuration and averaging [22–24,32,33].	Distributed strain and temperature	Range–resolution–acquisition trade-off. Strain–temperature cross-sensitivity; dual-end access for BOTDA
Rayleigh/OFDR	Local Rayleigh spectral correlation	Fully distributed. Millimeter-class sampling in selected OFDR systems, with concrete crack accuracy established by independent structural tests [58,70].	Strain fields, crack localization, local temperature	Range–resolution trade-off; correlation loss/decorrelation; high data volume
Raman DTS	Stokes/ anti-Stokes intensity relation	Distributed temperature. A concrete-dam configuration reported 1.02 m spatial and 0.5 °C temperature resolution with a minimum 10 s acquisition interval [59].	Temperature	Temperature measurement and compensation; calibration, averaging time, and signal-to-noise ratio govern the validated result.
Polymer optical fiber	Intensity, wavelength, backscatter, or deformation-dependent response	Discrete or distributed. Current systematic review identifies large-strain monitoring as a principal strength. Intensity-modulated sensing dominates reviewed SHM applications [12].	Large strain, deflection, crack opening, cumulative deformation	Higher attenuation; viscoelasticity/ hysteresis; temperature/humidity dependence
Fiber-optic chemical/durability sensors	Fluorescence, intensity, resonance, reflectance, or Raman response	Predominantly local. Selected distributed implementations, including ~0.5 m relative-humidity sensing [65].	pH, chloride, humidity, carbonation, corrosion state or corrosion-induced response	Selectivity/cross-sensitivity; response time; ageing/drift; calibration stability

Figure 2 groups the sensing principles and their main measurement characteristics. Its Rayleigh example refers specifically to OFDR, whose tens-of-meters operating range and millimeter-class spatial resolution do not characterize phase-sensitive OTDR or distributed acoustic sensing. Quantitative cross-family trade-offs are compared in Tables 2–4 and Figure 3.

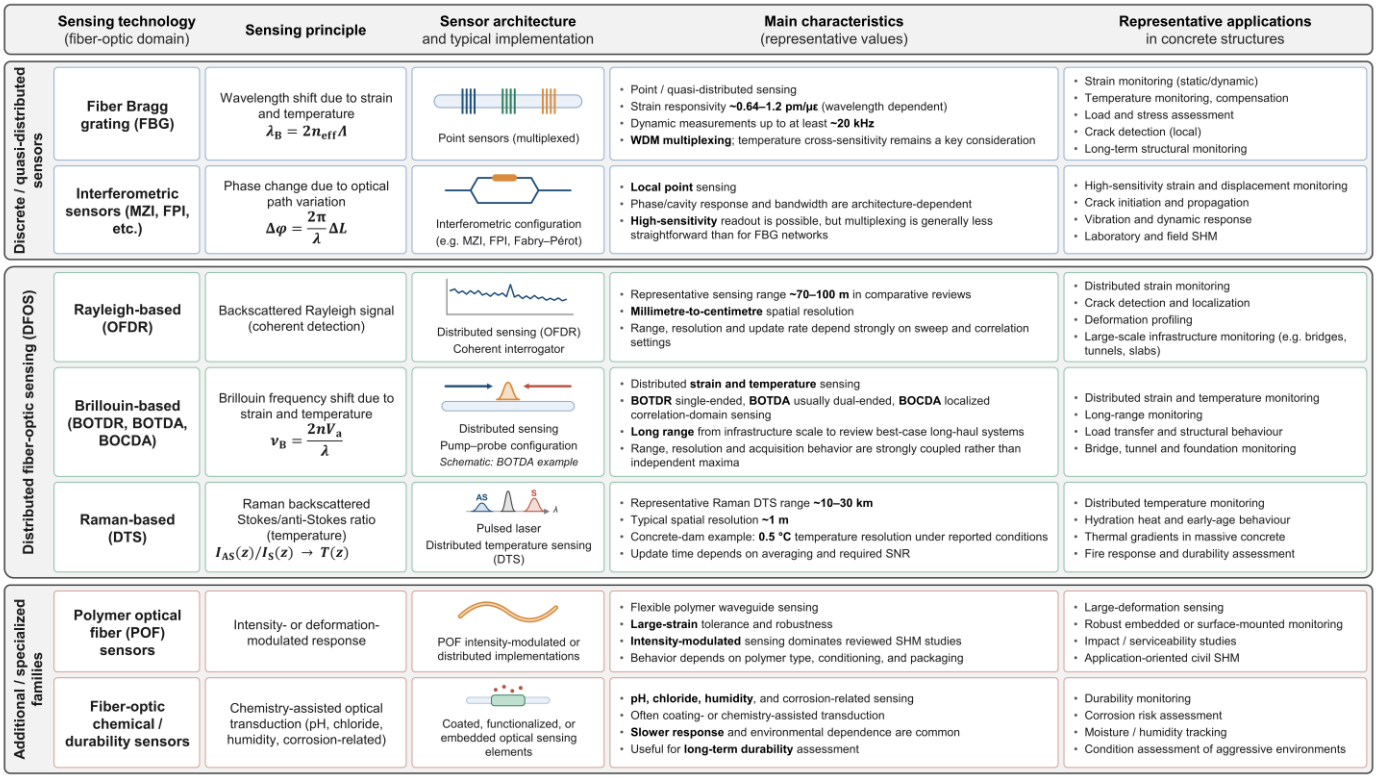


Figure 2. Main fiber-optic sensing approaches relevant to concrete SHM and representative values reported in the literature [5–7,12,20,22–24,29,30,59].

4. Interrogation and Sensor-Network Architectures

The sensing element alone does not determine the usable measurement capability of a fiber-optic SHM system. Interrogation architecture, wavelength or frequency allocation, optical power budget, acquisition strategy, and processing determine how sensor output is converted into a quantitative structural measurement. This section compares these system-level constraints for FBG, distributed, and hybrid optical networks.

4.1. FBG Interrogation, Multiplexing, and Long-Distance Networks

An FBG produces a wavelength-encoded response. The structural quantity is recovered after demodulation of the reflected spectrum. Interrogation is therefore an integral part of the measurement chain. Common approaches include broadband sources with spectrometers or array detectors, wavelength-scanning or tunable-filter methods, interferometric demodulation, and power-detection schemes using wavelength-dependent filters [5,7]. Their practical differences lie in wavelength resolution, acquisition rate, channel capacity, stability, optical power budget, and implementation complexity.

Filter-based interrogation can reduce hardware complexity. In an edge-filter arrangement, the FBG spectral shift is converted into an optical-power change on a calibrated spectral slope. The sensitivity and usable wavelength interval are linked directly, while source stability, detector linearity, and receiver sensitivity become part of the calibration [7]. Supe et al. [71] compared a filter/transceiver interrogator with a spectrometer reference

for mechanical strain measurements. Higher receiver sensitivity increased the usable measurement range and reduced noise, while the shorter-range transceiver remained suitable for continuous monitoring within a limited operating interval [71]. Filter-based readout is practical when the transfer function and operating range are defined for the intended measurement task.

Wavelength-division multiplexing places an additional constraint on FBG network design. Each grating must remain spectrally distinguishable over the expected strain and temperature excursion. The usable sensor count depends on source and interrogator bandwidth, FBG spectral width and side lobes, nominal channel spacing, expected Bragg shift, and the wavelength-estimation method [5,7]. Recent FBG interrogation work continues to emphasize the coupling between the optical readout architecture, spectral allocation, and the expected measurement range [7,71]. A channel grid that is adequate in the unloaded state can become insufficient when neighboring spectra broaden or shift toward one another. Wavelength allocation must therefore be defined together with sensor calibration and the expected operating range.

Long-distance FBG networks also depend on the optical power budget and network topology. The received level from each sensing point is affected by launch power, fiber attenuation, coupler and splitter losses, connector and splice losses, grating reflectivity, and receiver dynamic range. Murans et al. [72] examined FBG measurement lines extending to 50 km and showed that grating and network parameters must be considered jointly. The 50 km result represents a specific design case. Achievable distance changes with sensor count, topology, component losses, source power, and interrogator sensitivity. Large networks require optimization of the complete optical link rather than a single parameter such as grating reflectivity.

Grating spectral shape also affects network scalability. Murans et al. [72] compared Gaussian, sine, and raised-sine apodization and evaluated their influence on reflectivity, side-lobe suppression (SLS), and full width at half maximum (FWHM). Side-lobe suppression can improve separation between neighboring reflections, but the resulting bandwidth and peak reflectivity must still satisfy the wavelength and power requirements of the network [72]. For concrete SHM, the useful grating spectrum remains resolvable across the expected strain and temperature range while retaining sufficient reflected power.

Comparison of FBG networks depends on both sensor and interrogator parameters. Relevant descriptors include center wavelength, reflectivity, FWHM, apodization type, channel spacing, expected wavelength excursion, optical loss, wavelength-estimation method, wavelength uncertainty, temperature calibration, and the reference used to assess final strain. Optical scan rate and effective per-channel update rate after peak estimation, filtering, and averaging are different quantities. For dynamic work, the latter must be reported with the usable bandwidth and simultaneous channel count. Table 3 collects the corresponding descriptors for FBG and distributed architectures.

4.2. Distributed Interrogation and the Range–Resolution–Acquisition Trade-Off

Distributed systems cannot be compared using a nominal spatial-resolution value alone. In Brillouin- and Rayleigh-based sensing, the measured strain or temperature profile also depends on the interrogation method, spatial processing window, signal averaging, and demodulation procedure. Sensing range, output-point spacing, effective spatial resolution, acquisition or update time, and strain/temperature precision are treated as separate parameters [4,10,31,32]. Closely spaced output points do not necessarily represent independent measurements at the same spatial scale.

Brillouin systems can monitor strain and temperature over long fiber lengths, but sensing distance, spatial resolution, and the time needed to obtain a complete profile

depend on the interrogation settings [22–24]. In BOTDA and BOTDR, the interrogator measures the Brillouin spectrum along the fiber and fits its peak frequency. The peak shift is converted to strain or temperature using calibrated coefficients and, for mechanical strain, an independent temperature measurement or a calibrated method for separating the two responses [32,33]. In these time-domain systems, shorter pulses improve spatial resolution but reduce signal strength; spectral scanning and averaging affect the time between completed profiles [22,32]. BOTDR requires access to one fiber end, whereas BOTDA normally requires both. BOCDA selects a localized correlation peak for finer spatial measurement, with different sensing-length and update-time limits [11,22]. Table 3 sets out the distance, effective spatial resolution, frequency-fit uncertainty, and profile update time needed to compare specific configurations.

Rayleigh OFDR provides fine spatial resolution over shorter sensing lengths than long-range Brillouin systems. Current comparative reviews place coherent OFDR sensing in the tens-of-meters class, with approximately 70 m and millimeter-class spatial resolution reported as representative values in a 2025 review [23]. Other recent reviews place practical OFDR ranges broadly in the ~70–100 m class depending on implementation [23,24]. A tunable coherent source is swept over an optical-frequency interval, and local strain or temperature is recovered from changes in the Rayleigh signature [10,39–41]. Concrete measurements remain strongly configuration-dependent: Sieńko et al. reported resolution starting from 5 mm [42], while enhanced-Rayleigh laboratory studies illustrate how processing length and signal strength affect resolution and precision [31]. Source coherence, sweep linearity, optical-frequency sampling, detector performance, gauge length, and the correlation or spectral-estimation procedure must therefore be reported with the final structural quantity.

Interrogator settings directly affect crack-related measurements in concrete. A crack creates a localized deformation field that is transferred to the fiber and averaged over the optical processing length. The measured peak height and width depend on bonding, cable construction, processing length, and signal quality [8,42,43,57,70]. Crack width inferred by integrating the strain field also depends on the baseline, integration limits, and transfer or fitting model. The cited beam studies assessed crack-width estimates against independent digital image correlation measurements [58,70].

4.3. Hybrid Networks, Shared Optical Infrastructure, and Data Processing

Hybrid optical sensing is justified when the combined channels resolve an ambiguity that one channel cannot resolve alone. FBG and OFDR measurements have been used together in reinforced-concrete mock-ups to combine local FBG readings with distributed strain fields [51], while recent mass-concrete monitoring combines distributed strain and temperature information with explicit compensation to separate thermal and mechanical effects [33]. The benefit should therefore be demonstrated at the measurand level—for example, improved temperature separation, crack interpretation, spatial coverage, or redundancy—rather than inferred from the number of sensor types. Hybrid architectures also introduce synchronization, calibration-transfer, and data-fusion requirements that can offset the apparent advantage of additional sensing channels.

Shared optical infrastructure provides another integration route by carrying sensing and data-transmission functions in the same fiber plant. Coexistence of telecommunication services and cyclic FBG sensing has been demonstrated in a shared C-band passive optical network (PON) through wavelength and time allocation based on FBG spectral occupancy [73]. Senkans et al. [74] simulated a unified hybrid wavelength-division-multiplexed passive optical network (WDM-PON) with five FBG sensors over a 20 km transmission line. Integrating the sensing subsystem resulted in a reported power penalty below 0.5 dB at

the pre-forward-error-correction (pre-FEC) bit-error-rate (BER) criterion. Once sensing and communication share optical components, wavelength allocation, splitter and coupler losses, reflected sensor power, channel isolation, source spectrum, and receiver dynamic range affect both functions. Evaluating shared-fiber systems therefore requires considering sensing and communication metrics together.

Combining sensing technologies also introduces a time-alignment problem. FBG arrays, OFDR measurements, Brillouin scans, and durability sensors can operate with substantially different acquisition and averaging intervals [7,10,11]. Joint interpretation requires the time stamp, acquisition window, averaging procedure, and update rate of each channel to be retained. Resampling a slow distributed scan onto the time grid of a high-rate FBG channel does not make the measurements dynamically equivalent. Event-oriented SHM additionally requires a common time reference and a stated temporal uncertainty for each sensing channel.

Traceability from the raw optical response to the engineering quantity is central to data processing in SHM. Depending on the sensing principle, the processing chain can include FBG peak estimation, Brillouin-frequency fitting, Rayleigh spectral correlation, signal-quality checks, temperature compensation, filtering, drift correction, and conversion to strain, temperature, crack-related, or durability parameters. Machine-learning methods can then support anomaly detection, damage localization, severity assessment, environmental compensation, or prognosis. Current reviews identify limited labelled damage data, environmental variability, model transferability, and system-level integration as persistent constraints [2,75]. Recent work also places physics-informed and hybrid learning, uncertainty-aware modelling, and digital-twin integration among the emerging directions [75]. These methods do not remove the need for metrological traceability: a model trained on processed FOS data remains dependent on the sensing configuration, preprocessing, reference labels, and operating conditions used to generate those data. The corresponding comparison parameters are summarized in Table 3.

Table 3. Interrogation approaches and key parameters for sensor-system comparison.

Interrogation Approach	Measured Optical Quantity	Main Scalability Benefit	Key Comparison Parameters
Spectral/wavelength-scanning FBG interrogation	Bragg wavelength/reflected spectrum	Multiplexed wavelength-coded sensor arrays	Wavelength range and accuracy/resolution; scan/sampling rate; dynamic range; sensor count; peak-estimation algorithm; spectral spacing relative to expected Bragg shifts [5,7].
Filter/edge-filter FBG interrogation [7,71]	Optical power mapped through a calibrated wavelength-dependent transfer function	Lower hardware complexity; potentially high acquisition rate within a defined wavelength interval	Filter transfer function and slope; linear wavelength range; source stability; detector linearity, receiver sensitivity; calibration.
BOTDA/BOTDR	Brillouin frequency shift along fiber	Kilometer-scale distributed measurement	Range, sampling interval, effective spatial resolution, spectral-fit uncertainty, averaging, scan duration, and temperature separation [22–24,32,33].
BOCDA	Localized Brillouin correlation-peak frequency shift	Fine spatial selection in a correlation-domain measurement	Correlation-peak width and position, measurable length, scan/update time, frequency-fit uncertainty, strain–temperature separation, and independent reference [11,22].

Table 3. *Cont.*

Interrogation Approach	Measured Optical Quantity	Main Scalability Benefit	Key Comparison Parameters
Rayleigh OFDR	Local Rayleigh spectral shift/correlation	Dense high-resolution distributed measurement	Sensing length, output spacing, gauge pitch or processing length, signal quality, update rate, and independent crack/strain reference [58,70].
Raman DTS	Stokes/anti-Stokes intensity ratio	Long distributed temperature coverage	Calibration and reference thermometers, spatial resolution, temperature resolution versus accuracy, averaging, and effective update interval [59,60].
Hybrid/shared optical network	Several sensing observables and/or data-transmission channels in a common fiber plant	Complementary sensing and reduced duplicated optical infrastructure	Wavelength plan; shared components; optical budget; isolation/crosstalk; per-channel rate; synchronization. Hybrid WDM-PON/FBG example: 20 km with <0.5 dB reported power penalty [74].

5. Measurement Capabilities in Concrete Structures

Fiber-optic measurements in concrete are most informative when they are evaluated against the engineering quantity and decision task they are intended to support. The following subsections therefore distinguish direct optical measurands from derived structural quantities. Strain or temperature can be calibrated directly from wavelength, frequency, or spectral changes, whereas crack width, prestress loss, corrosion state, and damage severity usually require an additional mechanical, chemical, or statistical model. Quantitative examples are interpreted within their reported experimental conditions, distinguishing calibration performance from field accuracy.

5.1. Strain, Temperature, Prestress, and Early-Age Response

Strain and temperature are established measurands in fiber-optic monitoring of concrete, but the reported structural quantity depends on the measurement chain. FBG wavelength shifts and Brillouin frequency shifts are both affected by mechanical strain and temperature, and temperature also influences the interpretation of other distributed measurements. Long-term strain measurements require the raw optical response, temperature-compensation method, and mechanical strain reference state to be defined. Recent concrete studies demonstrate simultaneous distributed strain–temperature monitoring with explicit compensation in mass concrete [33], while other recent work integrates FBG and distributed sensing during curing and subsequent loading [76].

Temperature compensation can use a mechanically isolated reference FBG, a co-located temperature sensor, a loose or strain-decoupled reference fiber, separate strain- and temperature-sensitive distributed fibers, or a calibrated multiparameter procedure. The suitability of each method depends on the temperature range and monitoring duration. A constant-temperature assumption can be acceptable in a short, controlled loading test but is generally unsuitable for field or early-age monitoring. Experimental validation commonly applies a known temperature change under negligible mechanical loading and evaluates the residual apparent strain. Separate distributed strain and temperature channels have been used in dam monitoring [77], while a temperature-compensation coefficient was explicitly introduced for BOTDR measurements in a mass-concrete raft foundation [33].

Prestress monitoring can be based on different optical measurement concepts. Recent work has embedded optical fibers in epoxy-coated prestressing strands and used distributed sensing to estimate force and strain along the strand [28]. Long-gauge fiber-optic measurements have also been used to estimate long-term prestress losses from structural strain

changes [78], while FBG systems have been applied to reinforcing-bar slip and bond-slip characterization [25]. These approaches measure different physical quantities—local strand strain, distributed tendon strain, structural strain, or displacement—and should be compared using reference measurements that match the reported measurand, such as jacking force, load-cell data, or independent displacement.

Early-age monitoring is affected by the evolution of the strain reference state as concrete changes from a fresh to a hardened material. Recent work has shifted toward simultaneous distributed strain–temperature monitoring and explicit thermal compensation. Hou et al. developed a temperature-dependent compensation model for BOTDR and validated the approach in a mass-concrete raft foundation [33], while recent concrete FOS studies also demonstrate FBG and distributed-sensing integration during curing and subsequent loading [76]. Distributed sensing has been used to characterize shrinkage-induced strains in restrained concrete elements [48]. These studies emphasize a clearly defined time zero, coupling condition, temperature reference, compensation method, and distinction between apparent optical strain and mechanical deformation.

Long-term measurements place greater emphasis on repeatability, reference stability, drift, data continuity, and recovery of slow structural changes under environmental variation. Fernandez et al. [79] monitored reinforced-concrete beams with embedded Rayleigh-based distributed sensors for 96 days under sustained deflection and cyclic loading and validated strain, deflection, and derived crack width against independent measurements. Abdel-Jaber and Glisic [78] analyzed a seven-year field dataset from the post-tensioned Streicker Bridge. At the reported location, long-term prestress losses were approximately 8% of the total prestressing force, with more than half of that long-term loss occurring during the first six months. Imai [80] likewise reported seven years of Brillouin-based crack-detection monitoring. Monitoring duration is therefore itself a performance descriptor because short loading tests cannot establish multi-year stability of the reference state, sensor bond, or environmental compensation.

5.2. Crack Detection and Distributed Strain-Field Measurement

Distributed sensing is particularly useful for crack monitoring because it records a strain field without requiring the crack position to be predefined. Modern Rayleigh/OFDR systems can identify localized strain concentrations and thereby support crack detection and localization [19,40–42,52,53]. Current reviews describe the crack-monitoring problem as three distinct tasks: detecting crack initiation, locating the crack, and quantifying crack width or its evolution [8,19]. These tasks should not be collapsed into a single claim of ‘crack monitoring’. A system can detect a localized anomaly while still having insufficient strain transfer, signal quality, or spatial support for reliable crack-width estimation. The measured response near a crack is additionally influenced by sensing-cable construction, coating, bond, strain-transfer length, gauge length, and correlation quality [19,31,41,57,58].

Crack detection and crack localization are separate from the quality of the recovered strain peak. A crack may be identifiable from a local strain increase even when the peak shape is broadened, truncated, or partly decorrelated. Barrias et al. used a spectral-shift-quality metric to assess OFDR data in cracked reinforced-concrete beams [41], while comparative tests with several distributed fiber-optic sensing (DFOS) configurations showed clear differences in strain-peak shape and in crack widths derived from the same structural response [39,41,58]. A missing or broadened peak cannot be assigned only to structural behavior. Local signal quality and sensing configuration also have to be considered.

Crack-width estimation is a separate processing step. Rayleigh/OFDR studies have evaluated flexural cracks [40,42] and shear cracks using two-dimensional fiber layouts [43]. The integration of distributed strain requires a specified transfer length and a treatment

of background structural strain. Herbers et al. [58] compared five sensor types on two 4 m reinforced-concrete beams using digital image correlation (DIC) as the reference. The best robust cable showed a mean absolute width deviation of about 0.012 mm and a maximum deviation of 0.045 mm under that test configuration. In a separate 4 m beam study, changing the gauge pitch from 0.65 to 5.20 mm reduced the measurable strain gradient from about 1500 to 60 με/mm; at 2.60 mm, the tested combinations could not reliably assess openings above approximately 0.2 mm [70]. These are structural validation results, not interrogator specifications.

Two-dimensional and multilayer fiber arrangements extend a one-dimensional strain trace into a structural strain field. Orthogonal or grid layouts have been used to identify shear-crack patterns, calculate crack widths, and reconstruct principal and shear strains in reinforced-concrete D-regions [43,46,47]. These layouts are useful when crack orientation is not known in advance, because the result does not depend on one longitudinal fiber crossing the crack at a favorable angle. The reconstructed field can also show load-transfer paths and the development of disturbed regions that are not represented adequately by a small number of point sensors [46].

Distributed strain profiles have been compared with nonlinear finite-element predictions [44], while digital image correlation (DIC) has been used to inspect critical regions identified by distributed sensing and to validate crack-width estimates [50,58].

5.3. Durability Parameters and Chemical/Corrosion Sensing

Durability-oriented optical measurements quantify exposure, transport, chemical state, or corrosion-related response rather than structural safety directly. Fiber-optic pH, chloride, carbonation, and humidity sensors characterize conditions associated with reinforcement depassivation and corrosion risk [13–18,20,63–66]. Corrosion-sensitive coatings and probes respond to material changes associated with corrosion, while grating- or strain-based approaches can capture corrosion-induced deformation. Structural interpretation therefore requires a defined link between the optical response, the environmental or electrochemical state, and the damage mechanism.

Quantitative evaluation of durability sensors depends on calibration against the corresponding chemical or environmental measurand. Recent durability reviews emphasize calibration range, sensitivity or resolution, selectivity, packaging, environmental cross-sensitivity, and service-life considerations across FBG, LPFG, fluorescence, SPR, and distributed approaches [20]. In concrete-related primary studies, Tariq et al. [14] applied ratiometric fluorescence to hydroxide-diffusion measurements, while Fan et al. [18] demonstrated a fluorescent chloride probe in cement paste over 0.001–0.3 M, with a reported measurement error below 3% and a response time of about 6 s. These results illustrate why calibration accuracy, response time, and long-term stability must be reported separately. Earlier pH demonstrations [13] establish alkaline-range sensing principles, but their numerical results reflect the instruments and test conditions of those studies. Results obtained in pore solution or cement paste do not directly represent field accuracy after embedment in hardened concrete, where diffusion, local chemistry, functional-layer ageing, and temperature can modify the response.

Carbonation and moisture measurements operate on different spatial and temporal scales. Recent in situ carbonation work by Da Silva et al. [63] obtained a 1.6–18% reflected-intensity increase as $CaCO_3$ formed around an embedded multimode fiber and tested the concept under 3.2% CO_2. Chow et al. [65] reported an approximately 0.5 m distributed humidity sensing length, less than 1% RH difference between duplicate calibrated measurements, and used about 1 cm of fiber data for smoothing of the final humidity profile. Earlier Raman-based carbonation profiling [66] provides proof-of-principle evidence and

independent chemical validation. Its excitation and packaging parameters describe the tested configuration. Packaging required for embedment can modify moisture transport and response time [67]. Reliable interpretation therefore depends on the calibration range, response and recovery behavior, drift, exposure conditions, and an independent chemical or environmental reference.

Corrosion monitoring separates direct corrosion-sensitive transduction from measurement of corrosion-induced structural response. Zhou et al. [69] monitored a gold-sputtered long-period grating with an iron-carbon coating during 312 h in simulated concrete pore solution while collecting electrochemical data in parallel, while Luo et al. [68] reported a Fe-C-coated polymer-optical-fiber approach for steel-bar corrosion monitoring. Other optical approaches infer corrosion through strain, pressure, refractive-index, or coating changes associated with corrosion progression. Recent durability reviews and contemporary sensor implementations inform assessment of present-day capabilities [20,68,69]. Cross-study comparison should report exposure or acceleration conditions, sensor location, calibration relationship, independent corrosion reference, and whether the output represents initiation, progression, material loss, or corrosion-induced strain.

5.4. Dynamic and Event Sensing

Dynamic and event-oriented measurements occupy distinct frequency regimes. Structural vibration and modal-strain monitoring can be addressed by high-rate FBG interrogation, whereas acoustic-emission and stress-wave measurements generally require different transducer and interrogator architectures [81]. A recent civil-engineering FBG review reports vibration implementations extending to at least 20 kHz [6]. This is a configuration-specific system capability rather than an intrinsic bandwidth of the grating.

In dynamic FBG measurements, temporal performance is set mainly by the interrogator and processing chain. Channel count, wavelength-estimation method, sampling rate, synchronization, noise floor, and filtering determine which vibration or transient features can be reconstructed. FBG studies should therefore report bandwidth, sampling or update rate, strain/noise performance, and multiplexed-channel conditions instead of treating the sensing element alone as the dynamic-performance limit [5–7].

Acoustic-emission and stress-wave sensing operate at substantially higher frequencies than conventional structural-vibration monitoring. Their usable bandwidth is strongly architecture-dependent and cannot be transferred directly among interferometric, FBG, and cavity-based transducers [81]. Event-sensing performance should therefore be reported together with signal-to-noise ratio, transducer coupling, acquisition bandwidth, triggering or processing method, and the loading regime used for validation.

Long-term monitoring does not always require continuous acquisition at the maximum available rate. For event-triggered systems, the reporting protocol should define the trigger criterion, pre-trigger buffer, dead time, and retained waveform length, and event capture should be validated over the frequency and amplitude range relevant to the structural task. Continuous systems likewise require validation over the frequency and amplitude range relevant to the intended measurement. This differs from durability monitoring, where calibration stability and ageing over long periods are usually more important than bandwidth. Table 4 summarizes the monitoring quantities and quantitative validation items used to compare optical sensing approaches in concrete structures.

Table 4. Measurement tasks and quantitative validation items for optical sensing in concrete structures.

Monitoring Quantity	Most Relevant Optical Approach	Main Information Obtained	Validation Metric
Local strain/temperature	FBG	Local or quasi-distributed strain/temperature response	Wavelength coefficient, interrogator resolution and per-channel rate; calibrated strain error after thermal compensation and installation [5–7,71].
Distributed strain trend	Brillouin	Long-range strain/temperature profile	Profile error against a reference, temperature cross-sensitivity, cable transfer, scan time, and drift; report BOTDA, BOTDR, and BOCDA conditions separately [32,33].
Crack location/strain field	Rayleigh/OFDR	High-resolution strain concentration and field	Crack-location error against DIC or another independent reference, processing length, signal quality, and effective structural resolution [58,70].
Crack width	Rayleigh/OFDR with validated conversion	Estimated opening after localization and strain-field conversion	Crack-width error against DIC or a displacement reference, with transfer length and gauge pitch. In one two-beam comparison, the best robust sensor had ~0.012 mm mean absolute and 0.045 mm maximum deviation [58]; gauge-pitch limits are reported in [70].
Prestress/bond	FBG, Brillouin or other DFOS, or long-gauge FOS integrated with strand/reinforcement	Local or distributed tendon strain, prestress-force/loss estimate, slip or bond-related response	Force/slip error versus independent reference; transfer calibration; repeatability/hysteresis. Recent prestress applications include optical-fiber-instrumented strands with distributed strain/force measurement [28] and long-gauge fiber-optic monitoring of long-term prestress losses from structural strain changes [78].
Early-age response	FBG and/or distributed strain with co-located temperature measurement	Setting, hydration/thermal evolution, shrinkage, and restrained deformation	Time-zero/reference state; temperature measurement and compensation; baseline stability; strain-transfer validation. Recent field work includes distributed strain–temperature monitoring with temperature-dependent compensation in a mass-concrete raft foundation [33].
Durability environment/corrosion state	Functionalized fiber, Raman/reflectance probe, corrosion-sensitive optical coating, or FBG on reinforcement	pH, chloride, humidity, carbonation indicator, depassivation or corrosion response, or corrosion-induced strain	Matrix/exposure calibration; selectivity/cross-sensitivity; response/recovery; drift/ageing; independent chemical or electrochemical reference. Current examples include distributed RH monitoring with duplicate differences below 1% RH [65], Fe–C polymer-fiber corrosion monitoring [68], iron–carbon LPG monitoring of passivation/depassivation [69], and recent durability-review synthesis [20].
Dynamic/event response	High-rate FBG, fiber-optic acoustic-emission, or ultrasonic/stress-wave sensor	Modal strain/vibration, transient strain, acoustic-emission or stress-wave event	Effective per-channel rate, bandwidth, strain/noise floor, synchronization, and independent event reference. FBG vibration results up to 20 kHz are configuration-specific review values [6].

Figure 3 depicts representative operating regimes for the fiber-optic architectures. The BOCDA entry is compared with BOTDR and BOTDA in Section 4.2 and Table 3. Optical output spacing, processing length, and demonstrated structural resolution are distinguished in Sections 3.2 and 5.2.

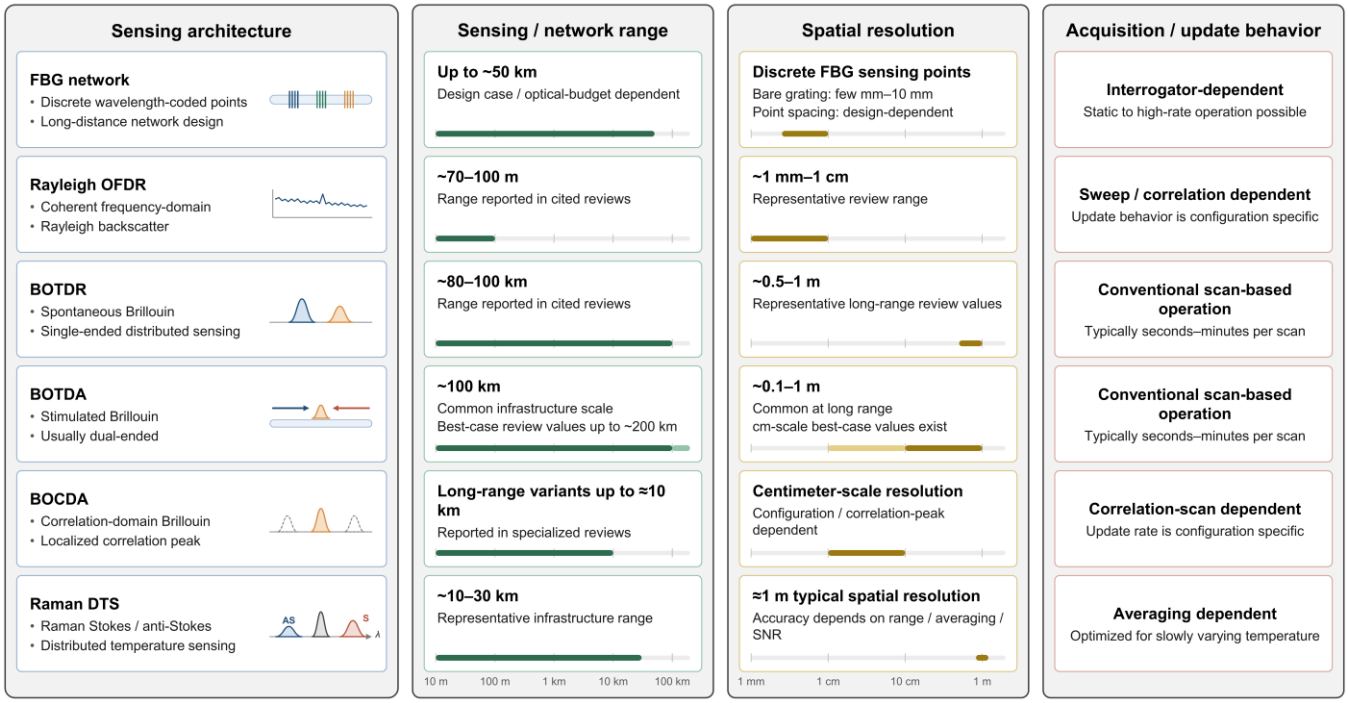


Figure 3. Representative sensing distances, spatial resolutions, and acquisition/update behavior for (a) an FBG network, (b) Rayleigh OFDR, (c) BOTDR, (d) BOTDA, (e) BOCDA, and (f) Raman DTS [6,7,11,22–24,72]. The ranges refer to different configurations. Table 3 and Section 5.2 identify the reporting conditions and independently validated concrete measurements. No panel combines the maximum range, finest resolution, and fastest rate as a single-system specification.

6. Publication and Terminology Trends in the Mapped Sensing Domain

The gathered and evaluated mapping describes publication-year counts and terminology in the specified technology and civil-infrastructure search domain. Some retrieved records concern non-concrete infrastructure. Interferometric, polymer-fiber, and chemical approaches were not separate query families, although their terms may occur in returned records.

6.1. Publication Growth and Technology Terminology Trends

The mapped source-record count rose from 145 in 2015 to 451 in 2025, a 3.1-fold difference between complete years. The annual series is 145 (2015), 152 (2016), 199 (2017), 206 (2018), 243 (2019), 193 (2020), 255 (2021), 252 (2022), 327 (2023), 359 (2024), and 451 (2025). It fell in 2020 and slightly in 2022, then rose each year from 2023 through 2025. The 318 records assigned to 2026 were indexed through 26 August and are shown separately from the complete-year comparison. Figure 4 shows the annual number of mapped Scopus records and non-exclusive occurrences of selected sensing-technology terms within the defined Scopus search domain.

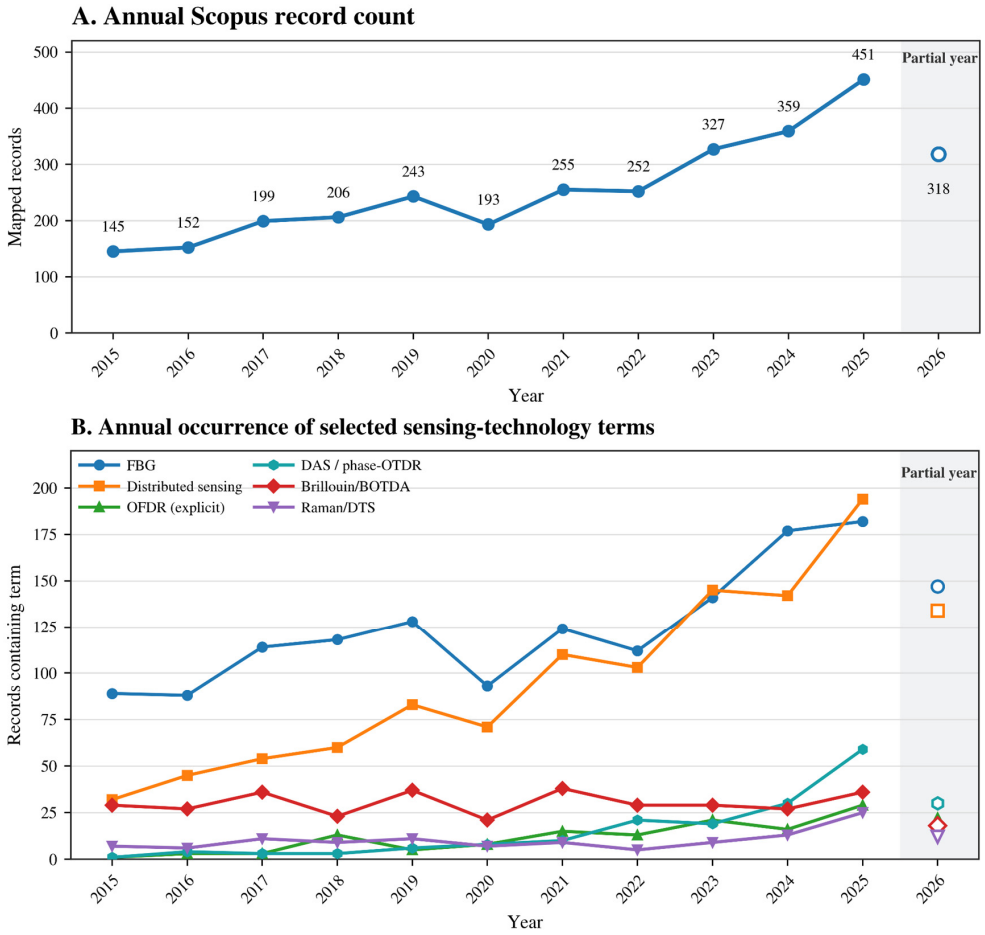


Figure 4. Annual counts of Scopus records and records containing selected sensing-technology terms (FBG, distributed sensing, OFDR (explicit), DAS/phase-OTDR, Brillouin/BOTDA, and Raman/DTS) in their titles, abstracts, or keywords within the Scopus mapping dataset. Term categories are non-exclusive, so a single publication may contribute to multiple categories. Data for 2026 cover only part of the year, as the records were indexed through 26 August 2026.

Journal articles account for 1982 mapped records (63.9%), conference papers for 979 (31.6%), reviews for 79 (2.5%), and book chapters for 60 (1.9%). Conference papers contribute a substantial part of the optics and photonics literature and help trace sensor, interrogator, and method development. Long-term stability, durability, and field-performance claims are assessed using studies that report the corresponding test duration and structural validation.

Across the 3100 mapped source records, the archived FBG, generic distributed-sensing, Brillouin/BOTDA, and Raman/DTS groups contain 1513, 1173, 350, and 124 records, respectively. The explicit OFDR and DAS/phase-OTDR flags introduced in Section 2.2 occur in 148 and 194 records. They may overlap with each other and with the archived groups. In 2015, OFDR wording occurred in 1 of 145 records (0.7%) and DAS wording in 1 of 145 (0.7%). In 2025, the respective counts were 29 of 451 (6.4%) and 59 of 451 (13.1%). FBG occurrences rose from 89 to 182, although their annual share fell from 61.4% to 40.4%. Generic distributed-sensing occurrences rose from 32 to 194 (22.1% to 43.0%). These are shifts in the wording of query-defined records and cannot establish corresponding growth in concrete deployments. As a scope check, 175 of the 451 records in 2025 explicitly contained concrete, cementitious, mortar, or grout in a title, abstract, or keyword field. However, broader search can also retrieve other civil-infrastructure settings.

The mapped literature is distributed across photonics, sensing, measurement, materials, and structural-engineering venues. The largest sources are *Sensors* (191 records; 6.2%), *Proceedings of SPIE—The International Society for Optical Engineering* (157; 5.1%), *Measurement* (108; 3.5%), *Engineering Structures* (82; 2.6%), and *Lecture Notes in Civil Engineering* (75; 2.4%), followed by *Construction and Building Materials*, *IEEE Sensors Journal*, *Optical Fiber Technology*, and structural-health-monitoring journals. This distribution reflects the close link between optical-system development and structural validation in the literature.

6.2. Evidence Levels and Comparability of Reported Results

For the evaluation, we propose three descriptive validation levels that are used for the selected primary studies, with the highest demonstrated level recorded for each example. Level 1 is controlled calibration of an optical or chemical response against the corresponding reference quantity, including tests in solution or cement paste [18,71]. Level 2 requires an installed sensor on a concrete specimen or realistic element and an independent measurement of the stated engineering quantity, such as strain gauges, displacement transducers, or DIC [41,58,70]. Level 3 documents operation on a field structure or over a sustained monitoring period with the reference state, exposure, and duration stated [33,77–80].

The validation levels describe how the sensing system was tested. Interpreting the reported result also requires distinguishing sensor sensitivity and interrogator resolution from the accuracy of the final measurement. For FBGs, the wavelength coefficient characterizes the optical response, whereas interrogator noise and strain transfer affect the measured strain [5–7,71]. Precision describes the consistency of repeated measurements, and accuracy is assessed against an independent reference. For OFDR crack measurements, output spacing alone does not determine the error in crack location or width on concrete [58,70].

Comparison across studies requires the sensing element or cable, installation, interrogator settings, processing interval, calibration and compensation, reference method, error metric, test scale, and observation duration to be reported together. A calibration error, change in the reference baseline over months, and disagreement with a structural reference are separate quantities. For chemically functionalized sensors, a solution or cement-paste calibration establishes Level 1 but not long-term accuracy after embedment in hardened concrete [18,20,69]. While Table 3 collects the reporting descriptors by interrogation method, Table 5 gives selected primary-study examples.

Table 5. Selected primary studies illustrating validation levels.

Technology/Source	Test and Reference	Reported Result	Level
FBG [71]	Two filter-based receiver configurations tested with 10 με micropositioner steps; spectrometer-type FBG interrogator used for comparison.	Reported operating range of approximately 150 με for receiver 1 and 200 με for receiver 2 in the tested configuration.	1
Rayleigh/OFDR [58]	Five fiber/cable types on two 4 m reinforced-concrete beams; crack widths referenced to DIC.	Best robust cable: ~0.012 mm mean absolute and 0.045 mm maximum crack-width deviation in the tested configuration.	2
Rayleigh/OFDR [70]	Calibration rig and 4 m reinforced-concrete beam in four-point bending; 0.65–5.20 mm gauge pitch; DIC reference.	Measurable gradient ~1500→60 με/mm as pitch increased; at 2.60 mm, the tested configurations lost reliable assessment above ~0.2 mm opening.	2

Table 5. *Cont.*

Technology/Source	Test and Reference	Reported Result	Level
BOTDR [33]	Temperature-compensation factor calibrated in a water bath from 20 to 70 °C in 5 °C steps; sensor layout tested on a reinforced-concrete beam against strain gauges; field monitoring of a mass-concrete raft from 18 April to 1 May.	The calibrated temperature-compensation factor K ranged from 1.26 to 2.67 over the tested temperatures and was applied during raft monitoring.	3 (field)
Raman DTS and thermal-field reconstruction [59]	Concrete-dam temperature monitoring during construction, with data analyzed through Day 28; Kriging-based reconstruction compared with three digital thermometers.	1.02 m spatial resolution; 0.5 °C temperature resolution; minimum 10 s acquisition interval. For the Kriging-reconstructed temperatures, mean absolute error was 0.75 °C and root mean square error was 0.96 °C against the three digital thermometers.	3 (field)
Raman DTS [60]	Full-scale facility with fiber embedded in concrete walls; temperature calibration against two Pt100 reference probes.	Expanded temperature uncertainty of 0.50–0.63 °C (95%) under the reported test conditions.	2
Chloride probe [18]	Fluorescent fiber probe calibrated against known chloride concentrations and tested for chloride ingress in cement paste.	0.001–0.3 M range; <3% reported error and ~6 s response under the study conditions.	1
Rayleigh/OFDR [79]	Embedded fiber in reinforced-concrete beams monitored for 96 days under sustained deflection and cyclic loading; comparison with DIC measurements.	Under cyclic loading, the mean error in deflection increments relative to DIC was below 5%. Crack-width increment differences were generally below 0.02 mm for the selected cracks, reaching 0.04 mm for one crack at higher loads.	3 (sustained lab. monitoring)

6.3. Interpreting Terminology Trends Alongside Validation Evidence

It is important to highlight that the Scopus layer records how often terms occur in a search-defined corpus. However, it does not measure how completely a sensing method has been validated. The previously combined Rayleigh/OFDR/DAS term count rose from 3 to 88 between 2015 and 2025, but the explicit split gives 1 to 29 for OFDR and 1 to 59 for DAS/phase-OTDR. The pooled count must therefore not be read as OFDR-specific growth. In the technical evidence, OFDR crack-width results vary with cable, bonding, processing length, and the transfer model: two beam studies used independent DIC references and reported different limits under their particular configurations [58,70]. FBG terminology increased from 89 to 182 records as its share of a growing corpus fell from 61.4% to 40.4%. Brillouin/BOTDA changed from 29 to 36 records, while cited Brillouin studies include temperature-compensated field monitoring [33] and long-duration crack detection [80].

Scopus counts therefore show how often sensing terms appear in the selected publications. The cited experiments are compared by the quantity measured (strain, temperature, crack location or width, pH, or chloride concentration), the sensor configuration, the independent reference measurement, and the reported error or uncertainty.

7. Research Gaps and Development Priorities

FBG networks need reports of usable channel count over the full strain–temperature excursion, spectral separation, optical power margin, per-channel update rate, and strain uncertainty after installation [5,7,71,72]. These descriptors are listed in Table 3 and should accompany concrete and road applications [27,82] rather than a sensor count alone.

Distributed strain measurements need cable, bond, gauge or processing length, signal quality, and an independent reference for the particular crack or strain quantity. The 0.65–5.20 mm gauge-pitch study [70] and the DIC comparison of five cable types [58] show why fine output spacing cannot substitute for a demonstrated crack-width error. Brillouin studies also need their range, spectrum-fitting conditions, temperature separation, and effective scan time reported together [32,33].

For chemical and corrosion sensors, the priority is stable calibration and selectivity after embedment, with ageing, temperature and wet–dry exposure, and an independent chemical or electrochemical reference [18,20,69]. Hybrid networks should show a measured benefit from the added channel, such as better thermal separation or more reliable structural interpretation [33,35,73,74]. Table 3 provides the corresponding system-reporting items.

Across these families, short calibration tests, concrete-element validation, and sustained field operation address different questions. Studies can be compared when their measurement configuration, final quantity, reference, error metric, and duration are explicit; the selected examples in Table 5 illustrate this distinction.

8. Conclusions

This review provides a common measurement-chain framework for comparing fiber-optic technologies used in concrete SHM. FBG systems provide multiplexed discrete or quasi-distributed measurements. Rayleigh/OFDR provides dense strain fields for crack localization and strain-field reconstruction. Brillouin methods extend distributed strain and temperature sensing over long distances. Raman DTS is primarily a distributed temperature technique, and polymer and functionalized optical sensors extend monitoring toward large deformation and durability-related measurands. Their capabilities are complementary and cannot be reduced to a single sensitivity, range, or spatial-resolution ranking.

The reviewed evidence shows that the final uncertainty depends on the complete chain: interrogation and thermal separation for FBG and Brillouin, bonding and processing length for OFDR crack measurements, and calibration stability and matrix effects for durability sensors. Table 3 specifies the reporting items needed to compare such results.

The three validation levels distinguish component calibration, independent assessment on concrete elements, and sustained or field operation. The primary-study examples in Table 5 show that these levels answer different questions, so a nominal sensor sensitivity or sampling pitch cannot stand in for an independently checked engineering result.

Within the specified Scopus search domain, annual source records rose from 145 (2015) to 451 (2025). FBG terminology rose in absolute count from 89 to 182, while its share fell from 61.4% to 40.4%. Generic distributed-sensing terminology rose from 32 to 194 records. Explicit OFDR wording rose from 1 to 29 records and DAS/phase-OTDR wording from 1 to 59, but these terms identify the vocabulary of retrieved publications, not concrete performance or deployment. The technical synthesis points instead to priorities in independently validated crack measurements, full-system FBG network reporting, temperature compensation, and long-duration assessment of durability sensors.

Supplementary Materials: The following supporting information can be downloaded at: https://www.mdpi.com/article/10.3390/photonics13121095/s1, Table S1 gives the exact Scopus queries,

export counts, reconciliation steps, and archived terminology groups. The explicit OFDR and DAS text-matching rules are defined in Section 2.2.

Author Contributions: Conceptualization, U.S. and J.B.; methodology, U.S. and J.B.; investigation, U.S., J.B., R.G. and A.S.; data curation, U.S. and J.B.; writing—original draft preparation, U.S., J.B., R.G. and A.S.; writing—review and editing, U.S., J.B., R.G. and A.S.; visualization, U.S. and J.B.; supervision, S.S. and V.B.; project administration, S.S. and V.B.; funding acquisition, S.S. and V.B. All authors have read and agreed to the published version of the manuscript.

Funding: The work was supported by the ERDF postdoctoral research project "Development of temperature and strain FBG sensor network for concrete construction monitoring solutions (FBG-SENS)" (Project No. 1.1.1.9/LZP/1/24/099).

Institutional Review Board Statement: Not applicable.

Informed Consent Statement: Not applicable.

Data Availability Statement: Supplementary Table S1 provides the search expressions and reconciliation details. Derived source-record fields used here (year, document type, internal record identifier, and technology-term flags) are available from the corresponding author upon reasonable request. Redistribution of Scopus bibliographic text and external identifiers remains subject to applicable licensing terms.

Conflicts of Interest: The authors declare no conflicts of interest.

References

1. Ansari, F. State-of-the-art in the applications of fiber-optic sensors to cementitious composites. *Cem. Concr. Compos.* **1997**, *19*, 3–19. [CrossRef]
2. Golovastikov, N.V.; Kazanskiy, N.L.; Khonina, S.N. Optical Fiber-Based Structural Health Monitoring: Advancements, Applications, and Integration with Artificial Intelligence for Civil and Urban Infrastructure. *Photonics* **2025**, *12*, 615. [CrossRef]
3. Masri, S.F.; Agbabian, M.S.; Abdel-Ghaffar, A.M.; Higazy, M.; Claus, R.O.; de Vries, M.J. Experimental study of embedded fiber-optic strain gauges in concrete structures. *J. Eng. Mech.* **1994**, *120*, 1696–1717. [CrossRef]
4. Senkans, U.; Silkans, N.; Spolitis, S.; Braunfelds, J. Comprehensive Analysis of FBG and Distributed Rayleigh, Brillouin, and Raman Optical Sensor-Based Solutions for Road Infrastructure Monitoring Applications. *Sensors* **2025**, *25*, 5283. [CrossRef] [PubMed]
5. Alhussein, A.N.D.; Qaid, M.R.T.M.; Agliullin, T.; Valeev, B.; Morozov, O.; Sakhabutdinov, A. Fiber Bragg Grating Sensors: Design, Applications, and Comparison with Other Sensing Technologies. *Sensors* **2025**, *25*, 2289. [CrossRef] [PubMed]
6. Yassin, M.H.; Farhat, M.H.; Soleimanpour, R.; Nahas, M. Fiber Bragg grating (FBG)-based sensors: A review of technology and recent applications in structural health monitoring (SHM) of civil engineering structures. *Discov. Civ. Eng.* **2024**, *1*, 151. [CrossRef]
7. Dey, K.; Majee, A.; Roy, S. Interrogation-Based Fiber-Optic Sensors: A Comprehensive Review of Techniques, Trends, and Applications. *IEEE Sens. Rev.* **2025**, *2*, 589–608. [CrossRef]
8. Xie, S.; Liu, Y.; Ansari, F.; Bao, Y. Distributed Fiber Optic Sensors for Monitoring Cracks in Civil Infrastructure. *Autom. Constr.* **2026**, *182*, 106717. [CrossRef]
9. Li, J.; Zhang, M. Physics and Applications of Raman Distributed Optical Fiber Sensing. *Light Sci. Appl.* **2022**, *11*, 128. [CrossRef] [PubMed]
10. Ding, Z.; Guo, H.; Liu, K.; Hua, P.; Zhang, T.; Li, S.; Liu, J.; Jiang, J.; Liu, T. Advances in Distributed Optical Fiber Sensors Based on Optical Frequency-Domain Reflectometry: A Review. *IEEE Sens. J.* **2023**, *23*, 26925–26941. [CrossRef]
11. Wang, Y.; Zhang, M. Recent Progress in Long-Range Brillouin Optical Correlation Domain Analysis. *Sensors* **2022**, *22*, 6062. [CrossRef] [PubMed]
12. Zhao, J.; Wang, J.; Zhou, W. Plastic Optical Fiber Sensors for Structural Health Monitoring: A Systematic Review. *Sens. Rev.* **2026**, *46*, 907–928. [CrossRef]
13. Nguyen, T.H.; Venugopala, T.; Chen, S.; Sun, T.; Grattan, K.T.V.; Taylor, S.E.; Basheer, P.A.M.; Long, A.E. Fluorescence based fibre optic pH sensor for the pH 10–13 range suitable for corrosion monitoring in concrete structures. *Sens. Actuators B Chem.* **2014**, *191*, 498–507. [CrossRef]
14. Tariq, A.; Ghasemi, R.; Lefevre, J.P.; Mongin, C.; Dauzères, A.; Leray, I. Ratiometric fiber optic fluorescent pH sensor for hydroxide diffusion measurements in concrete. *Sens. Actuators B Chem.* **2024**, *405*, 135297. [CrossRef]
15. Barrera, D.; Sales, S.; Cruz-Yusta, M.; Lozano, M.L.; Lloris, J.M.; Micó, V.; García-Olcina, R.; Esteve-Taboada, J.J.; Carrión, J.A.; López, M.J.; et al. Fiber Bragg Gratings for Measuring pH and Strain in Concrete Structures. *Proc. SPIE* **2008**, *7004*, 700444. [CrossRef]

16. Dhouib, M.; Conciatori, D.; Sorelli, L. Optical Fiber Chloride Sensor for Health Monitoring of Structures in Cold Regions. In *Proceedings of Cold Regions Engineering 2019, Reston, VA, USA, 2019*; American Society of Civil Engineers: Reston, VA, USA, 2019; pp. 391–397. [CrossRef]
17. Laferrière, F.; Inaudi, D.; Kronenberg, P.; Smith, I.F.C. Nouveau système de détection précoce des ions chlorure libres dans la solution interstitielle du béton: Capteur d'ions chlorure. *Eur. J. Environ. Civ. Eng.* **2009**, *13*, 283–303. [CrossRef]
18. Fan, L.; Ma, Z.; Liu, N.; Wan, Y.; Xiang, J.; Zhao, M. Development of alginate gel nanosphere-based fluorescent fiber optic sensor and its application in chloride ion monitoring of cement paste. *Cem. Concr. Compos.* **2026**, *165*, 106318. [CrossRef]
19. Zhang, X.; Long, L.; Broere, W.; Bao, X. Smart sensing of concrete crack using distributed fiber optics sensors: Current advances and perspectives. *Case Stud. Constr. Mater.* **2025**, *22*, e04493. [CrossRef]
20. Qiao, H.; Lin, Z.; Sun, X.; Li, W.; Zhao, Y.; Guo, C. Fiber Optic-Based Durability Monitoring in Smart Concrete: A State-of-Art Review. *Sensors* **2023**, *23*, 7810. [CrossRef] [PubMed]
21. Moser, D.; Martin-Candilejo, A.; Cueto-Felgueroso, L.; Santillán, D. Use of fiber-optic sensors to monitor concrete dams: Recent breakthroughs and new opportunities. *Structures* **2024**, *67*, 106968. [CrossRef]
22. Lv, B.; Peng, Y.; Du, C.; Tian, Y.; Wu, J. Review of Brillouin Distributed Sensing for Structural Monitoring in Transportation Infrastructure. *Infrastructures* **2025**, *10*, 148. [CrossRef]
23. Coscetta, A.; Catalano, E.; Damiano, E.; de Cristofaro, M.; Minardo, A.; Molitierno, E.; Olivares, L.; Vallifuoco, R.; Zeni, G.; Zeni, L. A Review of Strain-Distributed Optical Fiber Sensors for Geohazard Monitoring: An Update. *Sensors* **2025**, *25*, 6442. [CrossRef] [PubMed]
24. Taheri, S.; Siahkouhi, M.; Moghimi, A.; Rashidi, M. Distributed Fiber Optic Sensors (DFOSs) for Structural Health Monitoring (SHM) of Railway Infrastructure: A Critical Review. *Infrastructures* **2026**, *11*, 277. [CrossRef]
25. Pereira, L.; Mesquita, E.; Alberto, N.; Melo, J.; Marques, C.; Antunes, P.; André, P.S.; Varum, H. Fiber Bragg Grating Sensors for Reinforcing Bar Slippage Detection and Bond-Slip Gradient Characterization. *Sensors* **2022**, *22*, 8866. [CrossRef] [PubMed]
26. Braunfelds, J.; Senkans, U.; Skels, P.; Murans, I.; Porins, J.; Spolitis, S.; Bobrovs, V. Fiber Bragg Grating Optical Sensors for Road Infrastructure Monitoring Applications. In *Proceedings of Applied Industrial Optics 2022, Dublin, Ireland, 25–27 July 2022*; Optica Publishing Group: Washington, DC, USA, 2022. [CrossRef]
27. Senkans, U.; Silkans, N.; Merijs-Meri, R.; Skels, P.; Shaji, A.K.; Spolitis, S.; Haritonovs, V.; Braunfelds, J. Smart Road Infrastructure Enabled by Embedded FBG Sensor Network for Real-Time Structural Monitoring. In Proceedings of the 2025 Photonics & Electromagnetics Research Symposium—Fall (PIERS-Fall 2025), Chiba, Japan, 5–9 November 2025; IEEE: Piscataway, NJ, USA, 2025; p. 11394141. [CrossRef]
28. Williams, C.; Khatri, M.; Okumus, P.; Holt, R. Post-Tensioning Force Measurement Using Optical Fiber Sensor-Embedded Strand for Prestressed Concrete Structures. In *Building for the Future: Durable, Sustainable, Resilient—Proceedings of the Fib Symposium 2023, Volume 2*; Ilki, A., Çavunt, D., Çavunt, Y.S., Eds.; Springer: Cham, Switzerland, 2023; pp. 622–633. [CrossRef]
29. Yoo, J.W.; Kim, K.S.; Lee, T.G.; Lee, W.J.; Kim, J.W.; Kim, S.K. Embedded Intrinsic Fabry–Perot Optical Fiber Sensors in the Cement Concrete Structure for Health Monitoring System. In *Proceedings of Optical Fiber Sensors, Sapporo, Japan, 21–24 May 1996*; Optical Society of America: Washington, DC, USA, 1996. [CrossRef]
30. De Vries, M.; Arya, V.; Meller, S.; Masri, S.F.; Claus, R.O. Implementation of EFPI-based optical-fiber sensor instrumentation for the NDE of concrete structures. *Cem. Concr. Compos.* **1997**, *19*, 69–79. [CrossRef]
31. Loranger, S.; Gagné, M.; Lambin-Iezzi, V.; Kashyap, R. Rayleigh Scatter Based Order of Magnitude Increase in Distributed Temperature and Strain Sensing by Simple UV Exposure of Optical Fibre. *Sci. Rep.* **2015**, *5*, 11177. [CrossRef] [PubMed]
32. Senkans, U.; Silkans, N.; Spolitis, S.; Braunfelds, J. Recent Advances in Distributed Optical Sensing Technologies Based on Rayleigh, Brillouin and Raman Scattering. In Proceedings of the 2025 Photonics & Electromagnetics Research Symposium—Fall (PIERS-Fall 2025), Chiba, Japan, 5–9 November 2025; pp. 1–9. [CrossRef]
33. Hou, G.; Zhang, S.; Shao, Y.; Chen, H.; Bi, L.; Liu, H. Application of distributed optical fiber technology for strain and temperature monitoring in mass concrete raft foundations. *Opt. Fiber Technol.* **2026**, *96*, 104491. [CrossRef]
34. Okubo, K.; Imai, M.; Sogabe, N.; Nakaue, S.; Oikawa, M.; Chikiri, K. Monitoring on Tendon Force Distribution in Prestressed Concrete Bridge by Brillouin-Based Optical Fiber Sensor. In Proceedings of the 9th International Conference on Structural Health Monitoring of Intelligent Infrastructure (SHMII-9), St. Louis, MO, USA, 4–7 August 2019; pp. 659–664.
35. Mao, J.; Chen, J.; Cui, L.; Jin, W.; Xu, C.; He, Y. Monitoring the corrosion process of reinforced concrete using BOTDA and FBG sensors. *Sensors* **2015**, *15*, 8866–8883. [CrossRef] [PubMed]
36. Lanticq, V.; Quiertant, M.; Merliot, E.; Delepine-Lesoille, S. Brillouin Sensing Cable: Design and Experimental Validation. *IEEE Sens. J.* **2008**, *8*, 1194–1201. [CrossRef]
37. Alj, I.; Quiertant, M.; Khadour, A.; Grando, Q.; Benzarti, K. Environmental durability of an optical fiber cable intended for distributed strain measurements in concrete structures. *Sensors* **2022**, *22*, 141. [CrossRef] [PubMed]
38. Bado, M.F.; Casas, J.R.; Dey, A.; Berrocal, C.G. Distributed optical fiber sensing bonding techniques performance for embedment inside reinforced concrete structures. *Sensors* **2020**, *20*, 5788. [CrossRef] [PubMed]

39. Barrias, A.; Casas, J.R.; Villalba, S. SHM of reinforced concrete elements by rayleigh backscattering DOFS. *Front. Built Environ.* **2019**, *5*, 30. [CrossRef]
40. Rodríguez, G.; Casas, J.R.; Villalba, S. Cracking assessment in concrete structures by distributed optical fiber. *Smart Mater. Struct.* **2015**, *24*, 035005. [CrossRef]
41. Barrias, A.; Casas, J.R.; Villalba, S. Embedded distributed optical fiber sensors in reinforced concrete structures—A case study. *Sensors* **2018**, *18*, 980. [CrossRef] [PubMed]
42. Sieńko, R.; Zych, M.; Bednarski, Ł.; Howiacki, T. Strain and crack analysis within concrete members using distributed fibre optic sensors. *Struct. Health Monit.* **2019**, *18*, 1510–1526. [CrossRef]
43. Rodriguez, G.; Casas, J.R.; Villalba, S. Shear crack width assessment in concrete structures by 2D distributed optical fiber. *Eng. Struct.* **2019**, *195*, 508–523. [CrossRef]
44. Rodriguez, G.; Casas, J.R.; Villalba, S. Assessing Cracking Characteristics of Concrete Structures by Distributed Optical Fiber and Non-Linear Finite Element Modelling. In Proceedings of the 7th European Workshop on Structural Health Monitoring (EWSHM 2014), Nantes, France, 8–11 July 2014; pp. 1131–1138.
45. Berrocal, C.G.; Fernandez, I.; Bado, M.F.; Casas, J.R.; Rempling, R. Assessment and visualization of performance indicators of reinforced concrete beams by distributed optical fibre sensing. *Struct. Health Monit.* **2021**, *20*, 3309–3326. [CrossRef]
46. Fernandez, I.; Berrocal, C.G.; Rempling, R. Two-dimensional strain field analysis of reinforced concrete D-regions based on distributed optical fibre sensors. *Eng. Struct.* **2023**, *278*, 115562. [CrossRef]
47. Rodriguez, G.; Casas, J.R.; Villalba, S. Shear crack pattern identification in concrete elements via distributed optical fibre grid. *Struct. Infrastruct. Eng.* **2019**, *15*, 1630–1648. [CrossRef]
48. Bado, M.F.; Casas, J.R.; Dey, A.; Berrocal, C.G.; Kaklauskas, G.; Fernandez, I.; Rempling, R. Characterization of concrete shrinkage induced strains in internally-restrained RC structures by distributed optical fiber sensing. *Cem. Concr. Compos.* **2021**, *120*, 104058. [CrossRef]
49. Alj, I.; Quiertant, M.; Khadour, A.; Grando, Q.; Benzarti, K. Application of Distributed Optical Fiber Sensing Technology to the Detection and Monitoring of Internal Swelling Pathologies in Massive Concrete Blocks. *Sensors* **2022**, *22*, 7797. [CrossRef] [PubMed]
50. Morgese, M.; Domaneschi, M.; Ansari, F.; Cimellaro, G.P.; Inaudi, D. Improving distributed fiber-optic sensor measures by digital image correlation: Two-stage structural health monitoring. *ACI Struct. J.* **2021**, *118*, 91–102. [CrossRef]
51. Magne, S.; Rougeault, S.; Desmarchelier, R.; Chaudat, T.; Vasic, S.; Wang, F.; Hervé-Secourgeon, E.; Voldoire, F. In Situ Distributed Strain Monitoring of a Small-Scale Reinforced Concrete Structure Using Combined FBG/OFDR Fiber Optics Sensing for Assessment of Its Seismic Degradation Mechanisms. In Proceedings of the 12th International Workshop on Structural Health Monitoring (IWSHM 2019), Stanford, CA, USA, 10–12 September 2019; pp. 2557–2564. [CrossRef] [PubMed]
52. Richter, B.; Herbers, M.; Marx, S. Crack monitoring on concrete structures with distributed fiber optic sensors—Toward automated data evaluation and assessment. *Struct. Concr.* **2024**, *25*, 1465–1480. [CrossRef]
53. Tan, X.; Du, J.; Zhang, Q.; Meng, W.; Bao, Y. Monitoring restrained shrinkage and cracks of ultra-high-performance concrete (UHPC) using distributed fiber optic sensors. *Constr. Build. Mater.* **2024**, *422*, 135789. [CrossRef]
54. Li, J.; Yang, L.; Zuo, J.; Yang, R.; Zhang, X.; You, Y.; Kang, Y. Crack monitoring in cement mortar under impact loading using distributed optical fiber sensing. *Opt. Fiber Technol.* **2025**, *95*, 104386. [CrossRef]
55. Li, Z.-X.; Hou, G.-Y.; Hu, T.; Zhou, T.-C.; Xiao, H.-L. Study on establishing and testing for strain transfer model of distributed optical fiber sensor in concrete structures. *Opt. Fiber Technol.* **2021**, *61*, 102430. [CrossRef]
56. Barrias, A.; Casas, J.R.; Villalba, S. Distributed optical fibre sensors in concrete structures: Performance of bonding adhesives and influence of spatial resolution. *Struct. Control Health Monit.* **2019**, *26*, e2310. [CrossRef]
57. Billon, A.; Hénault, J.-M.; Quiertant, M.; Taillade, F.; Khadour, A.; Martin, R.-P.; Benzarti, K. Qualification of a distributed optical fiber sensor bonded to the surface of a concrete structure: A methodology to obtain quantitative strain measurements. *Smart Mater. Struct.* **2015**, *24*, 115001. [CrossRef]
58. Herbers, M.; Richter, B.; Gebauer, D.; Classen, M.; Marx, S. Crack Monitoring on Concrete Structures: Comparison of Various Distributed Fiber Optic Sensors with Digital Image Correlation Method. *Struct. Concr.* **2023**, *24*, 6123–6140. [CrossRef]
59. Xiang, Y.; Lin, P.; Peng, H.; Li, Z.; Liu, Y.; Qiao, Y.; Yang, Z. Optimization Method for Improving Efficiency of Thermal Field Reconstruction in Concrete Dam. *Appl. Sci.* **2024**, *14*, 10857. [CrossRef]
60. Houvin, M.; Moulouel, R.; Borel, P.; Boldo, D. Uncertainty Analysis and Metrological Validation of Raman Distributed Temperature Measurements in a Full-Scale Test Facility. *Sensors* **2026**, *26*, 2830. [CrossRef] [PubMed]
61. Schenato, L.; Bossi, G.; Marcato, G.; Pasuto, A. Cumulative monitoring of strain in concrete structures with polymer optical fibers. *Rend. Online Soc. Geol. Ital.* **2016**, *39*, 19–22. [CrossRef]
62. Ramani, V.; Kuang, K.S.C. Monitoring of rebar corrosion in concrete structures using a lens-based plastic optical fiber (LPOF) sensor. *Constr. Build. Mater.* **2021**, *276*, 122129. [CrossRef]
63. da Silva, P.M.; Mendes, J.P.; Coelho, L.C.C.; de Almeida, J.M.M.M. Real-Time Monitoring of Cement Paste Carbonation with In Situ Optical Fiber Sensors. *Chemosensors* **2023**, *11*, 449. [CrossRef]

64. Alustiza, D.H.; Mineo, M.; Arce, V.B.; Villa Pérez, C.; Russo, N.A. Experimental Fiber Optic Humidity Sensor with Applicability to Civil Structures Health Monitoring. *Opt. Pura Apl.* **2023**, *56*, 51138. [CrossRef]
65. Chow, C.W.K.; Rameezdeen, R.; Chen, G.Y.; Xu, H.; Rahman, M.M.; Ma, X.; Zhuge, Y.; Gorjian, N.; Gao, J. Real-Time Humidity Monitoring Using Distributed Optical Sensor for Water Asset Condition Assessment. *Water Conserv. Sci. Eng.* **2023**, *8*, 22. [CrossRef]
66. Yue, Y.; Wang, J.J.; Basheer, P.A.M.; Boland, J.J.; Bai, Y. A Raman spectroscopy based optical fibre system for detecting carbonation profile of cementitious materials. *Sens. Actuators B Chem.* **2018**, *257*, 635–649. [CrossRef]
67. Alustiza, D.H.; Russo, N.A.; Mineo, M.; López, A.; Villagrán-Zaccardi, Y.A. Packaging Design Assessment for an Experimental Fiber Optic Humidity Sensor Embeddable in Concrete Structures. In Proceedings of the 2022 IEEE Biennial Congress of Argentina (ARGENCON), San Juan, Argentina, 7–9 September 2022; pp. 1–4. [CrossRef]
68. Luo, D.; Li, Y.; Lim, K.-S.; Yang, H.; Ahmad, H. Development of Fe-C film coated polymer optical fiber sensor for steel bar corrosion monitoring. *Measurement* **2023**, *210*, 112561. [CrossRef]
69. Zhou, G.; Tang, F.; Li, G.; Li, H.-N. Gold-sputtered LPG fiber sensor pulse electroplated with iron-carbon for monitoring passivation and depassivation of carbon steel in concrete pore solutions. *Cem. Concr. Compos.* **2024**, *147*, 105432. [CrossRef]
70. Herbers, M.; Richter, B.; Marx, S. Rayleigh-based crack monitoring with distributed fiber optic sensors: Experimental study on the interaction of spatial resolution and sensor type. *J. Civ. Struct. Health Monit.* **2025**, *15*, 1439–1463. [CrossRef]
71. Supe, A.; Senkans, U.; Zurikovs, D.; Silkans, N.; Braunfelds, J. Mechanical Strain Monitoring Using Filter-Based Fiber Bragg Grating Interrogator. In Proceedings of the 2025 Photonics & Electromagnetics Research Symposium—Spring (PIERS-Spring 2025), Abu Dhabi, United Arab Emirates, 4–8 May 2025; pp. 1–9. [CrossRef]
72. Murans, I.; Braunfelds, J.; Senkans, U.; Spolitis, S.; Bobrovs, V. Designing of FBG Based Sensor Networks for Long-Distance Monitoring Solutions. In Proceedings of the 2023 Photonics and Electromagnetics Research Symposium (PIERS), Prague, Czech Republic, 3–6 July 2023; pp. 436–440. [CrossRef]
73. Cibira, G. Telecommunication Services and IoT FBG Sensing Shared in PON Optical Fiber Line. In *Proceedings of the 2021 Communication and Information Technologies (KIT), Vysoké Tatry, Slovakia, 13–15 October 2021*; IEEE: Piscataway, NJ, USA, 2021; pp. 1–5. [CrossRef]
74. Senkans, U.; Braunfelds, J.; Rubuls, K.; Murans, I.; Porins, J.; Bobrovs, V.; Spolitis, S. Development of Unified Hybrid WDM-PON With Spectrally Hidden Data Channel System and FBG Optical Sensor Network. *Latv. J. Phys. Tech. Sci.* **2023**, *60*, 99–103. [CrossRef]
75. Mahmood, Y.; Yasir, N.; Quenette, K.; Badin, G.; Huang, Y.; Xu, L. Fiber-Optic Sensor-Based Structural Health Monitoring with Machine Learning: A Task-Oriented and Cross-Domain Review. *Sensors* **2026**, *26*, 2641. [CrossRef] [PubMed]
76. Silkans, N.; Braunfelds, J.; Senkans, U.; Suta, M.; Fischer, G.; Spolitis, S. Fiber Optical Sensors Solutions for Concrete Construction Structural Health Monitoring. In Proceedings of the 2025 Photonics & Electromagnetics Research Symposium—Spring (PIERS-Spring 2025), Abu Dhabi, United Arab Emirates, 4–8 May 2025; IEEE: Piscataway, NJ, USA, 2025; pp. 1–11. [CrossRef]
77. Brezzi, L.; Schenato, L.; Cola, S.; Fabbian, N.; Chemello, P.; Simonini, P. Smart Monitoring by Fiber-Optic Sensors of Strain and Temperature of a Concrete Double Arch Dam. In *Geotechnical Engineering in the Digital and Technological Innovation Era*; Ferrari, A., Rosone, M., Ziccarelli, M., Gottardi, G., Eds.; Springer: Cham, Switzerland, 2023; pp. 161–168. [CrossRef]
78. Abdel-Jaber, H.; Glisic, B. Monitoring of Long-Term Prestress Losses in Prestressed Concrete Structures Using Fiber Optic Sensors. *Struct. Health Monit.* **2019**, *18*, 254–269. [CrossRef]
79. Fernandez, I.; Berrocal, C.G.; Rempling, R. Long-term performance of distributed optical fiber sensors embedded in reinforced concrete beams under sustained deflection and cyclic loading. *Sensors* **2021**, *21*, 6338. [CrossRef] [PubMed]
80. Imai, M. Seven-Year-Long Crack Detection Monitoring by Brillouin-Based Fiber Optic Strain Sensor. *Proc. SPIE* **2015**, *9435*, 94351Y. [CrossRef]
81. Willberry, J.O.; Papaelias, M.; Fernando, G.F. Structural Health Monitoring Using Fibre Optic Acoustic Emission Sensors. *Sensors* **2020**, *20*, 6369. [CrossRef] [PubMed]
82. Senkans, U.; Braunfelds, J.; Spolitis, S.; Bobrovs, V.; Porins, J. Analysis of FBG Based Sensing for Infrastructure Structural Health Monitoring Applications. In Proceedings of the 2023 Photonics and Electromagnetics Research Symposium (PIERS), Prague, Czech Republic, 3–6 July 2023; pp. 744–753. [CrossRef]

Disclaimer/Publisher's Note: The statements, opinions and data contained in all publications are solely those of the individual author(s) and contributor(s) and not of MDPI and/or the editor(s). MDPI and/or the editor(s) disclaim responsibility for any injury to people or property resulting from any ideas, methods, instructions or products referred to in the content.